Taylor, B., Fujioka, K., et al., 1990
Proceedings of the Ocean Drilling Program, Initial Reports, Vol. 126

6. SITES 788/789[1]

Shipboard Scientific Party[2]

HOLE 788A

Date occupied: 28 April 1989

Date departed: 28 April 1989

Time on hole: 12 hr, 45 min

Position: 30°55.35′N, 140°00.27′E

Bottom felt (rig floor; m, drill-pipe measurement): 1111.0

Distance between rig floor and sea level (m): 10.50

Water depth (drill-pipe measurement from sea level, m): 1100.5

Total depth (rig floor; m): 1156.30

Penetration (m): 45.30

Number of cores (including cores with no recovery): 5

Total length of cored section (m): 45.30

Total core recovered (m): 1.24

Core recovery (%): 3

Oldest sediment cored:
Depth (mbsf): 45.30
Nature: pumiceous pebbly vitric sand and vitric sand
Age: Quaternary

HOLE 788B

Date occupied: 28 April 1989

Date departed: 28 April 1989

Time on hole: 5 hr

Position: 30°55.38′N, 140°00.17′E

Bottom felt (rig floor; m, drill-pipe measurement): 1113.0

Distance between rig floor and sea level (m): 10.50

Water depth (drill-pipe measurement from sea level, m): 1102.5

Total depth (rig floor; m): 1148.60

Penetration (m): 35.60

Number of cores (including cores with no recovery): 4

Total length of cored section (m): 35.60

Total core recovered (m): 0.00

Core recovery (%): 0

Oldest sediment cored:
Depth (mbsf): 35.60
Nature: no recovery

HOLE 788C

Date occupied: 13 May 1989

Date departed: 14 May 1989

Time on hole: 1 day, 2 hr

Position: 30°55.36′N, 140°00.21′E

Bottom felt (rig floor; m, drill-pipe measurement): 1113.0

Distance between rig floor and sea level (m): 10.50

Water depth (drill-pipe measurement from sea level, m): 1102.5

Total depth (rig floor; m): 1375.50

Penetration (m): 262.50

Number of cores (including cores with no recovery): 28

Total length of cored section (m): 258.50

Total core recovered (m): 146.15

Core recovery (%): 56

Oldest sediment cored:
Depth (mbsf): 262.50
Nature: nannofossil clast
Age: Pliocene
Measured velocity (km/s): 2.42

HOLE 788D

Date occupied: 14 May 1989

Date departed: 16 May 1989

Time on hole: 1 day, 9 hr, 15 min

Position: 30°55.37′N, 140°00.22′E

Bottom felt (rig floor; m, drill-pipe measurement): 1113.0

Distance between rig floor and sea level (m): 10.50

Water depth (drill-pipe measurement from sea level, m): 1102.5

Total depth (rig floor; m): 1487.00

Penetration (m): 374.00

Number of cores (including cores with no recovery): 16

Total length of cored section (m): 154.40

Total core recovered (m): 12.28

Core recovery (%): 8

Oldest sediment cored:
Depth (mbsf): 374.00
Nature: vitric siltstone and vitric sandstone
Age: early Pliocene
Measured velocity (km/s): 2.61

HOLE 789A

Date occupied: 29 April 1989

Date departed: 29 April 1989

Time on hole: 8 hr, 45 min

Position: 30°55.24′N, 139°59.84′E

Bottom felt (rig floor; m, drill-pipe measurement): 1128.5

Distance between rig floor and sea level (m): 10.50

Water depth (drill-pipe measurement from sea level, m): 1118.0

Total depth (rig floor; m): 1182.60

[1] Taylor, B., Fujioka, K., et al., 1990. *Proc. ODP, Init. Repts.*, 126: College Station, TX (Ocean Drilling Program).
[2] Shipboard Scientific Party is as given in the list of participants preceding the contents.

Penetration (m): 54.10

Number of cores (including cores with no recovery): 6

Total length of cored section (m): 54.10

Total core recovered (m): 0.10

Core recovery (%): 0.2

Oldest sediment cored:
Depth (mbsf): 54.10
Nature: pumice
Age: Pliocene-Quaternary

Principal results: Sites 788 and 789 are located on the eastern margin of the Sumisu Rift between the active Izu-Bonin arc volcanoes Sumisu Jima (58 km north) and Tori Shima (55 km south-southeast). The sites are just over 0.5 km apart and are situated on the summit of the rift-flank footwall uplift, which is cut by high-angle normal faults dipping away on both sides from Site 788. The principal objectives of these sites were to determine (1) the vertical-motion history of the rift margin; (2) the time of initial rifting; and (3) the nature and history of volcanism and sedimentation between the major arc volcanoes. Site selection was made on the basis of multichannel seismic (MCS) records and a short shipboard seismic survey; the sites chosen lie on *Fred Moore* 3507, Line 4, at 2138Z (Site 788) and at 2133Z (Site 789). Sites 788 and 789 were occupied from 0030 hr (all times given in UTC), 28 April, to 0400 hr, 29 April; Site 788 was reoccupied from 1620 hr, 13 May, to 0330 hr, 16 May 1989.

Hole 788A was spudded at 0755 hr on 28 April 1989, rotary coring 45.3 m with 1.24 m of recovery. After offsetting 100 m northwest, four RCB cores were taken in Hole 788B, penetrating 35.6 m with zero recovery. The hole began to cave in and so was abandoned at 1820 hr on 28 April. Hole 789A was spudded at 2005 hr on 28 April, rotary coring 54.1 m with only 0.1-m recovery. Further coring was deferred until after drilling Sites 790 and 791. Hole 788C was spudded at 2144 hr on 13 May, and APC cored from 4 to 248.2 m below seafloor (mbsf) with 60% recovery. The hole was continued with extended core barrel (XCB) coring to 262.5 mbsf with 1% recovery before the pipe became stuck. After we freed the pipe, the string was tripped. Hole 788D was spudded with RCB coring at 0035 hr on 15 May and drilled with a center bit to 219.6 mbsf. Coring continued to 374 mbsf with 8% recovery. Because we had met our primary scientific objectives, we ended coring in the hole so that we would not jeopardize another bottom-hole assembly (BHA).

Two lithologic units were defined at Site 788:

1. Unit I (0–249 mbsf) is upper Quaternary and Pliocene sandy, granule and pebble, pumiceous gravel locally interbedded with vitric sands and rare vitric silts. There is a transition to the basal 20 m, which is a subunit (IB) lithified to conglomerate.
2. Unit II was divided into two subunits: Subunit IIA (249–277.6 mbsf) is Pliocene, interbedded nannofossil-rich claystone and vitric sandstone, silty claystone, and siltstone, moderately burrowed; and Subunit IIB (277.6–374 mbsf) is lower Pliocene, interbedded pumiceous conglomerate and vitric sandstone, siltstone, and silty claystone.

At Site 789, 0.1 m of Pliocene-Quaternary pumice was recovered from the surficial core.

Units I and II were dated by means of nannofossils, foraminifers, and paleomagnetics. There is an unconformity at about 30 mbsf between pumice less than 275 Ka and pumice 2.35–3.56 Ma. Pliocene sedimentation rates are >140 but <240 m/m.y. in Unit I and average 140 m/m.y. in Unit II, varying between as low as 40 m/m.y. in Subunit IIA and up to 280 m/m.y. in Subunit IIB. Benthic foraminifers indicate a depositional water depth of 1500–3000 m for Subunit IIA sediments.

The sediments are dominantly arc-derived volcaniclastic rocks, mostly pumiceous gravel and conglomerate. No igneous rocks were recovered. The silt/clay component and all biogenic materials were virtually absent in the coarse clastic rocks (carbonate is <0.5% in Unit I), probably as a result of winnowing. Carbonate-rich sections such as in Subunit IIA and middle Subunit IIB reflect slower deposition during volcanic minima lasting up to 300 k.y. Upward-coarsening intervals in Unit I represent four large eruptions, or four periods during which volcanism built up to climaxes, three in the Pliocene and one in the late Quaternary. The pumice is mainly rhyolitic, although the lower two cycles have more diverse clast types, including high-silica andesite.

Bedding is horizontal in Unit I to subhorizontal in Unit II. A zone of 30°–60° normal faulting occurs near 297 mbsf. Lithification was caused by compaction and pressure-welding in Subunits IB and IIA, plus carbonate and local zeolite cementation in Subunit IIB. The degree of compaction suggests that the overburden was formerly greater than at present.

Physical property measurements indicate that (1) average bulk density values increase from 1.5 g/cm^3 in Unit I to 2.0 g/cm^3 in Unit II; (2) porosity values range from 50%–90% (average 73%) in Unit I to 45%–70% (average 60%) in Unit II; and (3) sonic velocity data average 1.6 km/s in Unit I, 2.7 km/s (ranging from 2.4 to 3.3 km/s) in Subunit IIA, and 2.8 km/s (ranging from 2.0 to 3.4 km/s) in Subunit IIB.

The principal results of these sites are (1) the arc-margin footwall of Sumisu Rift has been uplifted between 200 and 1700 m; (2) the footwall uplift, and therefore the initiation of rifting, occurred since 2.35–3.56 Ma; (3) present-day and pre-rift volcanism and sedimentation along the volcanic front is dominated by rhyolitic pumice eruptions; and, (4) unlike other arcs such as Japan and the Cascades, there is no evidence at this site of igneous vents or lava flows between the large frontal-arc volcanoes during the last 5 m.y.

BACKGROUND AND OBJECTIVES

Site 788 is located at 30°55.36′N, 140°00.21′E, at 1102 m below sea level (mbsl), and Site 789 is located at 30°55.24′N, 139°59.84′E, at 1118 mbsl. Both sites are on the eastern margin of the Sumisu Rift between the active Izu-Bonin arc volcanoes Sumisu Jima (58 km north) and Tori Shima (55 km south-southeast; Figs. 1 and 2). The submarine arc caldera South Sumisu is 35–40 km to the north. The sites are just over 0.5 km apart and are located on the summit of the rift-flank footwall uplift (Figs. 2–4). The section is cut by active normal faults dipping ~45° away from Site 788 (Fig. 4). By drilling in the arc margin of the rift, we sought to determine (1) the vertical-motion history of the rift margin, (2) the time of initial rifting, and (3) the nature and history of volcanism and sedimentation between the major arc volcanoes.

The first of these objectives was addressed through a combination of paleontological estimates of paleobathymetry, backstripping the sedimentation history using the physical property and logging data, and seismic stratigraphic analyses of the interconnecting MCS profiles. The second objective was obtained by dating the unconformity resulting from the uplift of the rifted arc margin, assuming that the footwall uplift is a flexural and isostatic response to the unloading of the hanging wall block (Weissel and Karner, 1989). To meet the third objective required recovery, dating, and characterization of the upper part of the more than 1.5-km-thick margin section. The frequency, chemistry, and eruptive style of the pre-rift volcanism was ascertained from studies of the volcaniclastic sediments encountered.

Although the nature of the frontal-arc material between the arc volcanoes was unknown, analogy with such land sections as those in Japan or the Cascades suggested that there should be numerous vents and flow fields between the large volcanic edifices. Samples collected during an ALVIN dive indicate that the lower eastern rift wall consists of interbedded volcaniclastic rocks, pumice, and basalt (Taylor et al., in press). However, potential-field and sidescan marine geophysical data suggest a paucity of volcanic centers between the large edifices in the central Izu-Bonin intraoceanic arc.

SEISMIC STRATIGRAPHY

Correlation of MCS site survey data with recovered core material (Fig. 5) was accomplished by using physical properties velocity data, averaged over each lithologic unit (see "Physical

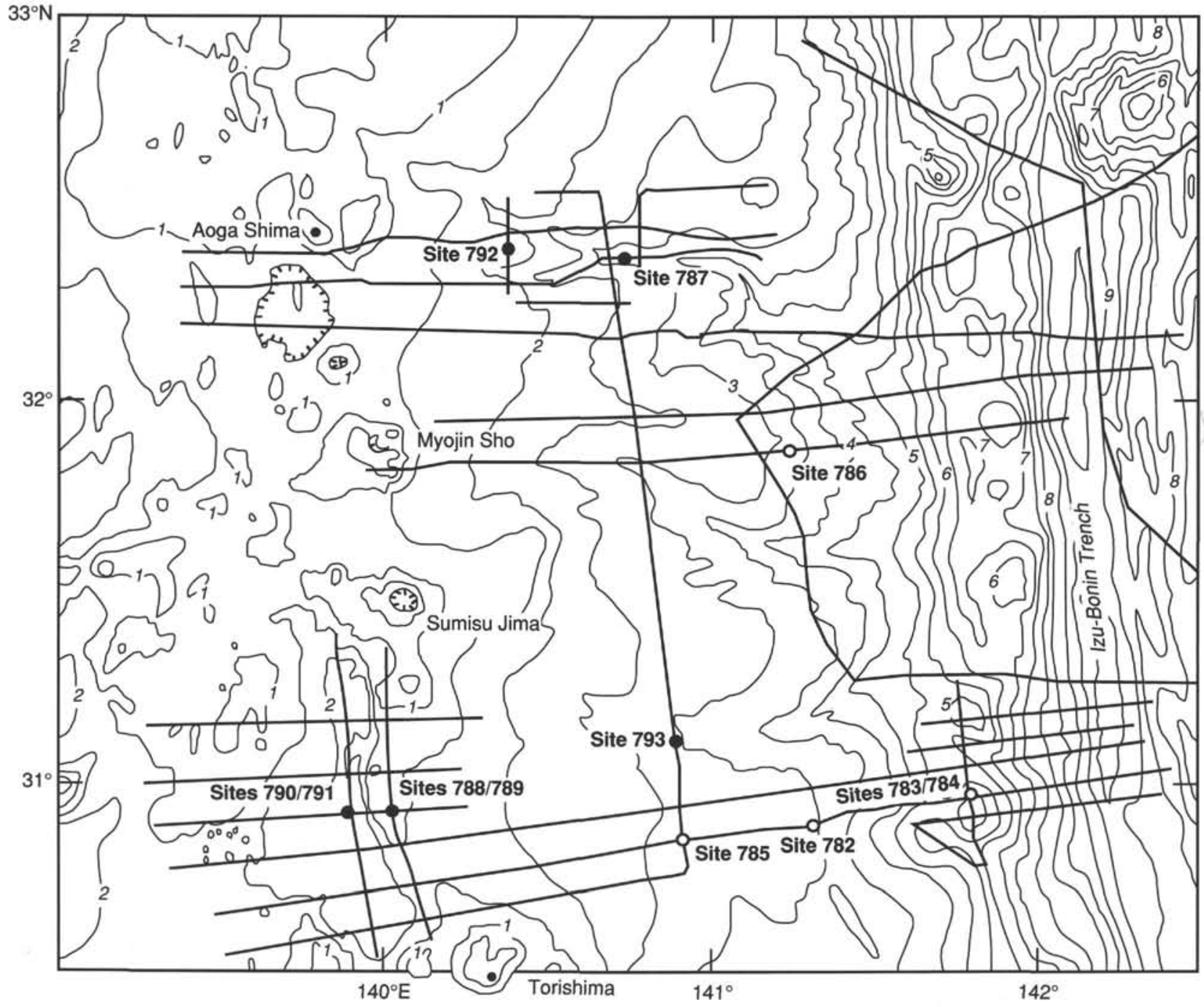

Figure 1. Bathymetric map, at 0.5-km contour intervals, of the Izu-Bonin arc-trench system between 30.5°N and 33°N. The locations of sites drilled on ODP Legs 125 (open circles) and 126 (filled circles) are shown on the map, as are the locations of MCS site survey lines.

Properties" section, this chapter), to convert depths (mbsf) into two-way traveltimes. The entire seismic section is characterized by relatively continuous reflectors observed down to multiple and is cut by active normal faults dipping away on either side of Site 788. Site 789, drilled to 54.1 mbsf, did not even pass through the seismic bubble pulse. At Site 788, Unit I is characterized by horizontal, slightly discontinuous, low-amplitude reflectors. The Unit I/II boundary correlates with a high-amplitude reflector (at 1.77 s). The large impedance contrast caused by the change from conglomerate (Subunit IB) to nannofossil claystones (Unit II) is responsible for generating this high-amplitude event. This reflector can be traced locally throughout this rift-flank uplift.

Unit I appears to be conformably deposited on this reflector at Site 788, but appears to be disconformable beneath Site 789. Unit II is characterized by discontinuous, low-amplitude reflections. Below the bottom of Site 788, a series of high-amplitude, well-layered reflectors are observed down to the water-bottom multiple reflection. It is inferred from the character of these reflectors that they represent sedimentary strata and that acoustic basement is not observed in the >1000 m of seismically imaged section.

OPERATIONS

Site 787 to Site 788

Before departing from Site 787, the televiewer (TV) umbilical cable detorquing procedure was conducted. A dead weight was attached to the TV cable and lowered to 3000 mbsl. As we slowly reeled in the cable, the ship drifted away from a point directly over the weight and the cable became angled in such a way that it dragged against the edge of the moonpool, resulting in eight lost strands over an interval of 2635–2850 m of paid-out cable. The remainder of the cable was recovered without further incident, and it was checked and found to have proper electrical continuity. Although the cable looked bad and spooled poorly, it was serviceable for the remainder of the leg.

The ship departed the site at 1200 hr on 27 April 1989 and arrived at Site 788 (proposed Site BON-2) with a routine beacon drop at 0030 hr on 28 April.

Site 788

The beacon was dropped near what appeared to be a fault, so the ship was offset 100 m from the beacon location along bearing 060° to place the hole as far as possible from the sus-

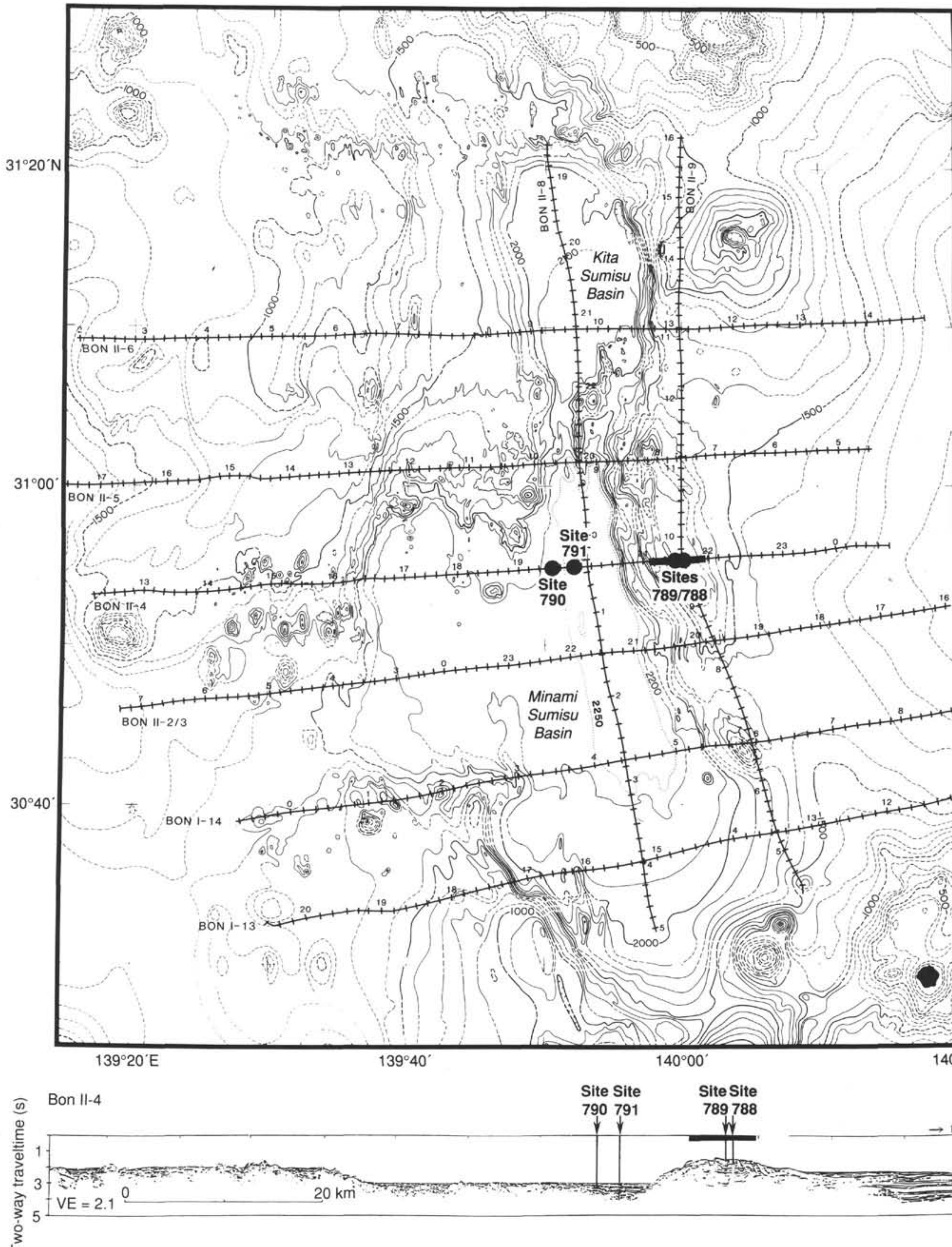

Figure 2. Bathymetric map (100-m contour intervals) of Sumisu Rift and surrounding area showing the location of MCS site survey tracks and of Sites 788–791. A line drawing of MCS Line BON II-4 (*Fred Moore* 35-07) is shown at the bottom of the figure. The segment of this line shown in Figure 4 is indicated by the solid bars in the upper and lower parts of the figure.

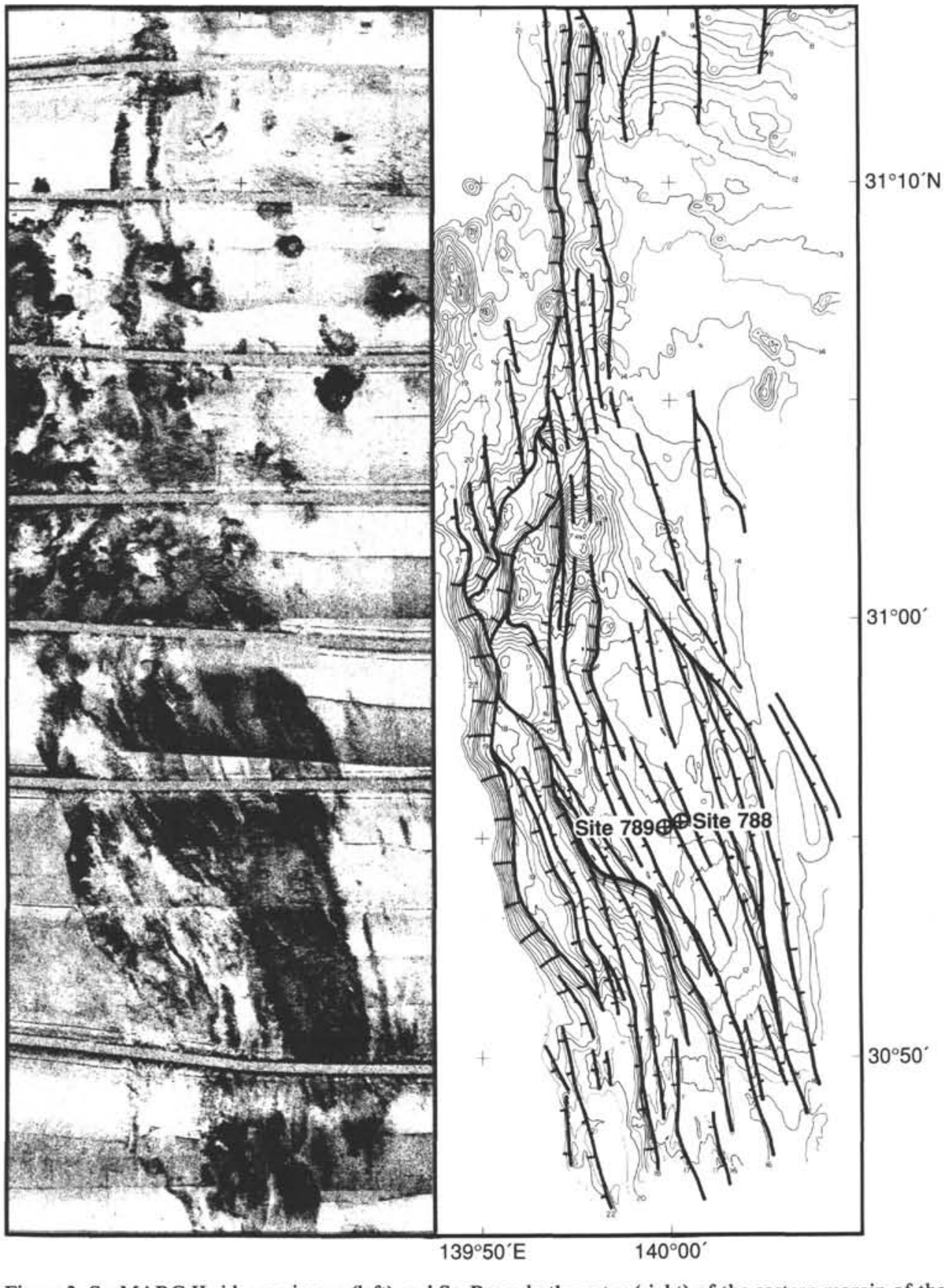

Figure 3. SeaMARC II sidescan image (left) and SeaBeam bathymetry (right) of the eastern margin of the Sumisu Rift showing the anastomosing and relay pattern of normal faults (from Taylor et al., in press) and the location of Sites 788 and 789.

pected fault. The precision depth recorder (PDR) water depth was 1112 mbsl.

Hole 788A

A new RCB BHA was put together and lowered slowly until contact with a very firm mud line was felt 1111 m below rig floor at 0755 hr. No penetration was possible without slight drill-pipe rotation, so a jet-in test was voided. The material near the surface of the formation behaved like loose sand, and this suspicion was strengthened by the fact that four of the first five core barrels were empty (Table 1). After recovering only 1.24 m of loose, pebbly sand in the upper 45 m of penetration, the hole was declared undrillable. The hole was abandoned, and the pipe cleared the seafloor at 1315 hr on 28 April 1989.

Hole 788B

The ship was moved to a new location 100 m due north of the beacon to try another spud, in the hope of finding at least some sediment or cohesive material. The results were again disappointing. Virtually identical circumstances prevailed, and four cores were taken without any recovery. After penetrating 35.6 m, the hole began to exhibit signs of caving in, and some overpull was necessary to free the pipe. The hole was abandoned at 1820 hr on 28 April.

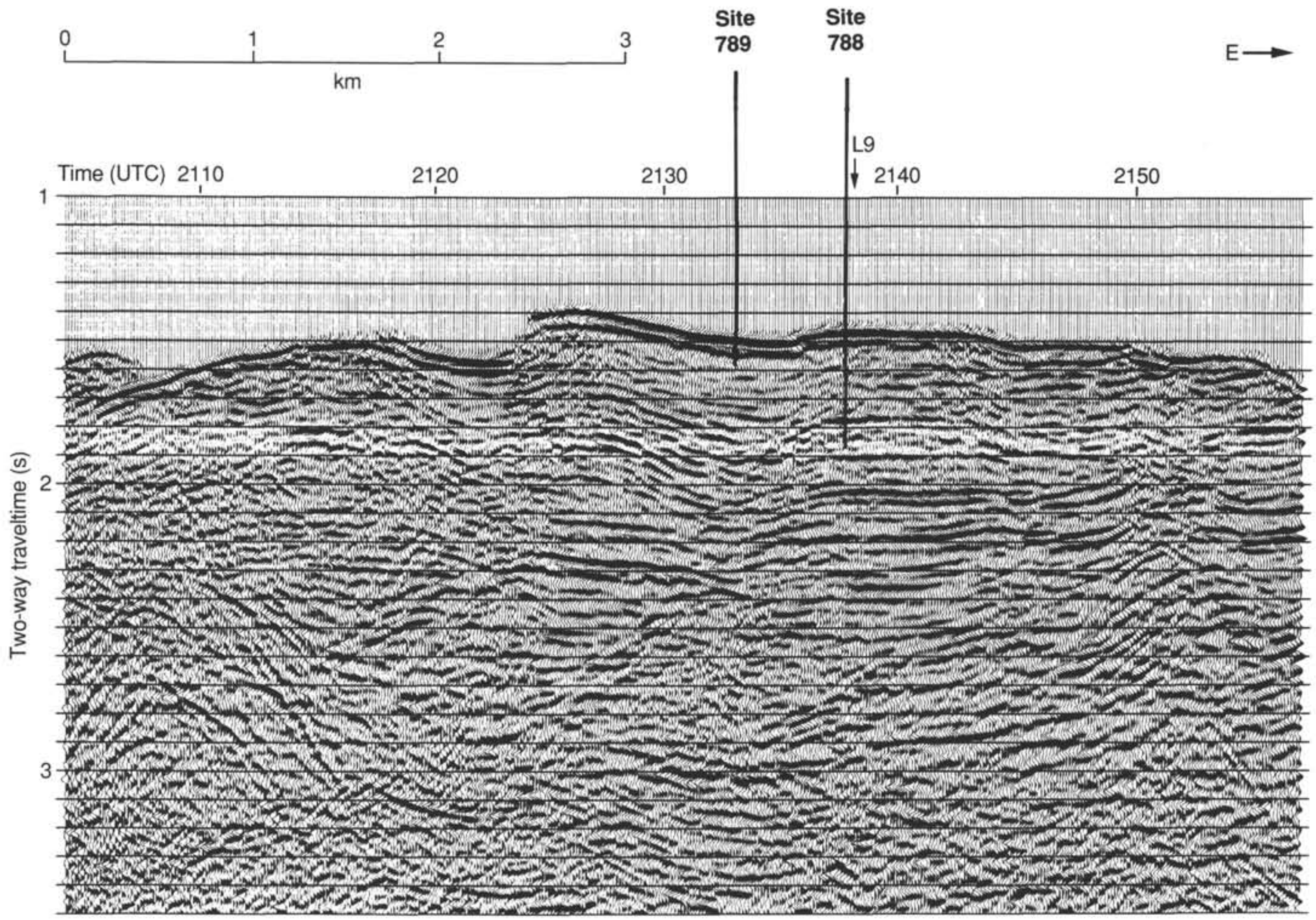

Figure 4. Latitudinal MCS profile BON II-4 (Taylor et al., this volume) across the eastern footwall uplift of the Sumisu Rift at 30°55′N (see Fig. 2 for location). Sites 788 and 789 are located on the summit of the uplift where the MCS data indicate a stratigraphic thickness greater than 1.5 km. The section is cut by active normal faults that dip at ~45° away from the central block into which Site 788 was drilled.

Site 789

Hole 789A

The ship was offset to a location of a shallow sediment pond where conditions at the seafloor might allow for some sediment recovery and better hole stability. The move was beyond beacon range, so a separate beacon was dropped and a new site designated. The hole was spudded 1128.5 m below rig floor at 2005 hr on 28 April. Six RCB cores were taken with only traces of recovery. After experiencing a 50,000-lb overpull to lift the pipe at a sub-bottom depth of only 54.1 m, the hole was declared undrillable and abandoned. The string was pulled and the bit was on deck at 0400 hr, 29 April.

Return to Site 788

The original attempts to core at Site 788 had been with the RCB coring system. Recovery, after four to five cores in very loose sand and gravel, had been essentially nil and the site was declared uncorable since it was thought that the APC also would fare poorly in the incompressible vitric material. Surprising success in piston coring in similar material at Sites 790 and 791 demonstrated that the APC was a viable coring approach after all. Armed with this new knowledge, the vessel returned in dynamic positioning mode to the still-active beacon at Site 788.

Hole 788C

A six-collar XCB BHA was assembled with a 10½-in., five-cone bit, and the pipe was run to the seafloor. The hole was spudded with the first shot being taken from a point 4 m below the mud line to avoid any chance of repeating the buckled core-barrel problem experienced at Hole 791A. The piston-coring results were successful and continued until Core 126-788C-26H at a depth of 248.2 mbsf, where APC refusal was defined by the lack of penetration in apparently firm, granular material. The XCB coring system was then applied for two core attempts, but problems ensued. During the piston-coring sequence, sand or cuttings had infiltrated the BHA and plugged off the five 14/32-in. bit nozzles.

Because of the obstruction, the flow to the bit was channeled entirely into the cutting-shoe flow path on the XCB core barrel. Core 126-788C-27X was declared a misrun when the cutting-shoe inner-flow sleeve collapsed completely because of high nozzle pressures and blocked the throat of the core barrel. Core 126-788C-28X was attempted at very low flow rates in an at-

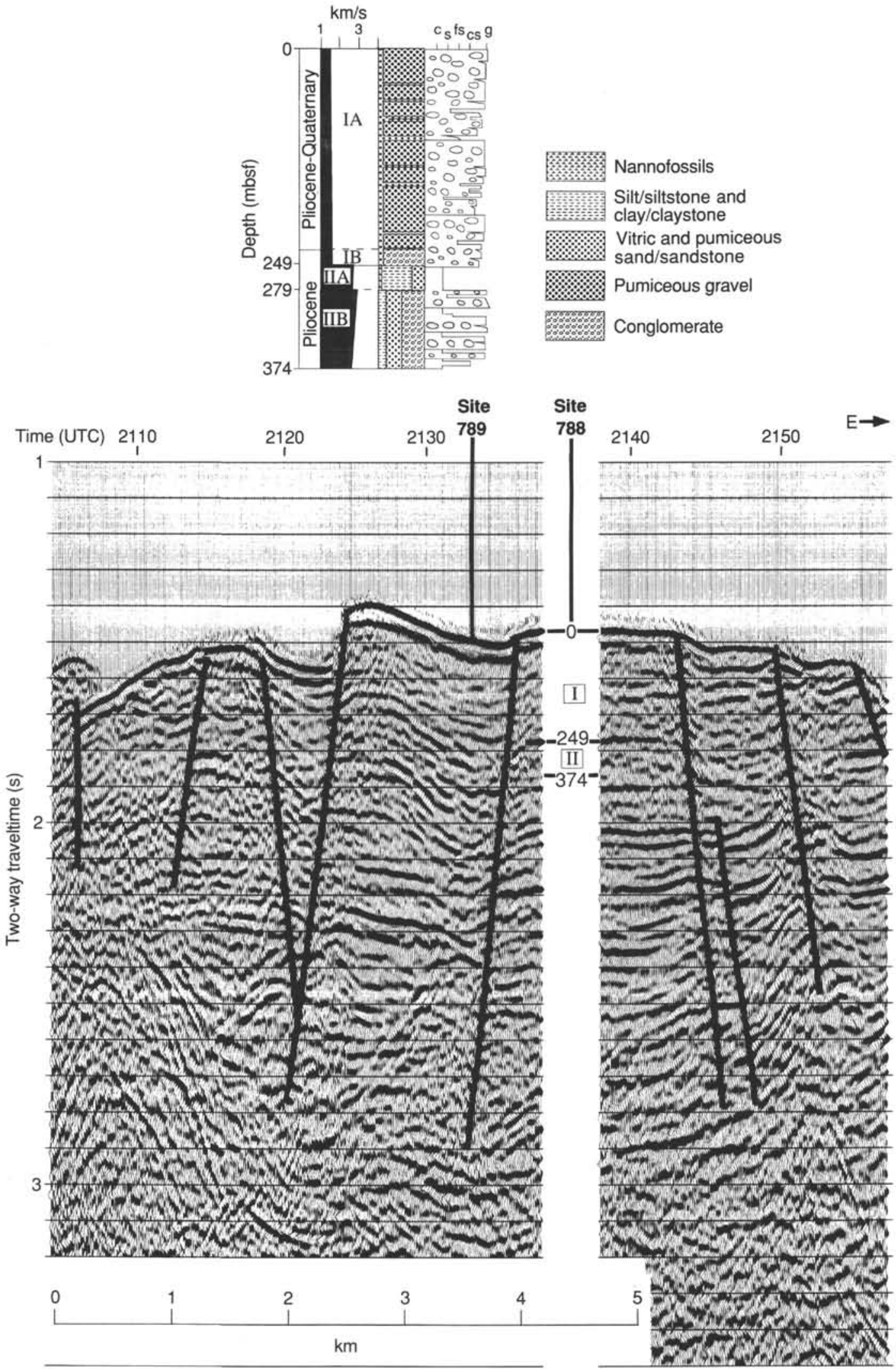

Figure 5. Correlation of Site 788 lithostratigraphy with MCS site survey data. Lithologic units are identified on the seismic section, unit boundaries are given in meters below seafloor (mbsf), and the lithologic column (see "Lithostratigraphy and Accumulation Rates" section, this chapter) is presented above the seismic section. The location of the *Fred Moore* seismic line is shown in Figure 2. The seismic profile has been stacked (48 fold), deconvolved, migrated, and filtered from 10 to 60 Hz. The vertical exaggeration is ~4×.

Table 1. Coring summary, Sites 788 and 789.

Core no.	Date (1989)	Time (UTC)	Depth (mbsf)	Cored (m)	Recovered (m)	Recovery (%)
Hole 788A:						
1R	Apr 28	0845	0-7.0	7.0	0	0
2R	Apr 28	0945	7.0-16.6	9.6	0	0
3R	Apr 28	1030	16.6-26.2	9.6	0.01	0.1
4R	Apr 28	1115	26.2-35.8	9.6	1.23	12.8
5R	Apr 28	1225	35.8-45.3	9.5	0	0
Coring totals				45.3	1.24	2.7
Hole 788B:						
1R	Apr 28	1455	0-7.0	7.0	0	0
2R	Apr 28	1600	7.0-16.5	9.5	0	0
3R	Apr 28	1640	16.5-26.0	9.5	0	0
4R	Apr 28	1715	26.0-35.6	9.6	0	0
Coring totals				35.6	0	0
Hole 788C:						
1H	May 13	2110	4.0-13.3	9.3	5.17	55.6
2H	May 13	2150	13.3-20.2	6.9	0.98	14.2
3H	May 13	2240	20.2-29.7	9.5	9.34	98.3
4H	May 13	2330	29.7-39.2	9.5	5.48	57.7
5H	May 14	0000	39.2-48.7	9.5	8.89	93.6
6H	May 14	0025	48.7-58.2	9.5	9.08	95.6
7H	May 14	0050	58.2-67.7	9.5	3.65	38.4
8H	May 14	0125	67.7-77.2	9.5	3.52	37.0
9H	May 14	0150	77.2-86.7	9.5	9.35	98.4
10H	May 14	0210	86.7-96.2	9.5	8.99	94.6
11H	May 14	0235	96.2-105.7	9.5	6.40	67.3
12H	May 14	0310	105.7-115.2	9.5	9.15	96.3
13H	May 14	0355	115.2-124.7	9.5	9.18	96.6
14H	May 14	0425	124.7-134.2	9.5	8.92	93.9
15H	May 14	0455	134.2-143.7	9.5	4.21	44.3
16H	May 14	0525	143.7-153.2	9.5	3.06	32.2
17H	May 14	0600	153.2-162.7	9.5	9.00	94.7
18H	May 14	0650	162.7-172.2	9.5	4.63	48.7
19H	May 14	0720	172.2-181.7	9.5	8.78	92.4
20H	May 14	0750	181.7-191.2	9.5	3.56	37.5
21H	May 14	0820	191.2-200.7	9.5	2.30	24.2
22H	May 14	0845	200.7-210.2	9.5	1.41	14.8
23H	May 14	0915	210.2-219.7	9.5	5.12	53.9
24H	May 14	0940	219.7-229.2	9.5	5.17	54.4
25H	May 14	1010	229.2-238.7	9.5	0.35	3.7
26H	May 14	1035	238.7-248.2	9.5	0.28	3.0
27X	May 14	1210	248.2-257.9	9.7	0.00	0.0
28X	May 14	1245	257.9-262.5	4.6	0.18	3.9
Coring totals				258.5	146.15	56.5
Drilled interval = 4.0 m						
Total penetration and recovery				262.5	146.15	56.5
Hole 788D:						
1R	May 15	0910	219.6-229.2	9.6	0.79	8.2
2R	May 15	1000	229.2-238.9	9.7	0.19	2.0
3R	May 15	1055	238.9-248.5	9.6	0.20	2.1
4R	May 15	1205	248.5-258.2	9.7	1.15	11.8
5R	May 15	1315	258.2-267.9	9.7	1.90	19.6
6R	May 15	1410	267.9-277.5	9.6	0.75	7.8
7R	May 15	1505	277.5-287.2	9.7	2.03	20.9
8R	May 15	1605	287.2-296.9	9.7	0.69	7.1
9R	May 15	1715	296.9-306.5	9.6	1.32	13.7
10R	May 15	1815	306.5-316.0	9.5	0.37	3.9
11R	May 15	1900	316.0-325.6	9.6	0.77	8.0
12R	May 15	1950	325.6-335.3	9.7	0.43	4.4
13R	May 15	2040	335.3-345.0	9.7	0.25	2.6
14R	May 15	2140	345.0-354.7	9.7	0.14	1.4
15R	May 15	2230	354.7-364.3	9.6	0.58	6.0
16R	May 15	2340	364.3-374.0	9.7	0.72	7.4
Coring totals				154.4	12.28	8.0
Drilled interval = 219.6 m						
Total penetration and recovery				374.0	12.28	8.0
Hole 789A:						
1R	Apr 28	2100	0-8.5	8.5	0.10	1.2
2R	Apr 28	0021	8.5-18.0	9.5	0	0
3R	Apr 28	2245	18.0-27.5	9.5	0	0
4R	Apr 28	2330	27.5-37.1	9.6	0	0
5R	Apr 29	0000	37.1-46.6	9.5	0	0
6R	Apr 29	0045	46.6-54.1	7.5	0	0
Coring totals				54.1	0.10	0.2

tempt to reduce the nozzle back pressure. The combination of low flow levels and the unstable formation caused the hole to collapse in the vicinity of the BHA and the pipe became stuck. Repeated overpulls of 260,000 lb freed the string after about 30 min. With the bit nozzles plugged and the hole deteriorating, the only choice was to pull out of the hole. The bit was on deck at 1815 hr on 14 May 1989, ending Hole 788C.

Hole 788D

In the final XCB core of Hole 788C (cut short by the hole collapse and stuck pipe), a sample of material representing a significant change in lithology was recovered. This, plus the possibility of still more lithology alternations nearby, dictated that the scientific goals of the hole were not quite accomplished. Thus, an RCB BHA was made up and run back to the seafloor. Hole 788D was spudded at 0035 hr on 15 May and drilled with a center bit to 219.6 mbsf. We took 16 RCB cores and then ended the hole at 374 mbsf. Recovery was poor but adequate enough to satisfy the first-order scientific objectives. The hole was abandoned and the bit was on deck after the pipe trip at 0330 hr on 16 May 1989.

LITHOSTRATIGRAPHY AND ACCUMULATION RATES

Introduction

Sites 788 and 789 are located atop the east flank of the Sumisu Rift graben. Site 789, 0.5 km southwest of Site 788, was cored with the RCB coring system. Penetration was 54.1 m, and only 0.1 m of pumiceous gravel was recovered (Section 126-789A-1R-CC) and received by the paleontology laboratory before the hole and the site were abandoned. This discussion is based principally upon the more successful results of APC and XCB coring of Hole 788C, and RCB coring of Hole 788D. Recovery was reasonably good in Hole 788C. The top of Hole 788D overlapped the basal portion of the 788C column, but recovery from Hole 788D was poor.

The stratigraphic succession at Site 788 consists of two lithologic units (Table 2 and Fig. 6), both of which are overwhelmingly dominated by volcanogenic components, much of it gravel and conglomerate. No igneous basement rock was recovered. Biogenic materials are virtually absent in the upper unit, and in the lower unit they are fairly abundant within only one interval. The contact between Units I and II was not recovered in Hole 788C but was recovered at 249 mbsf in Hole 788D. Table 3 summarizes the recovery of sediments and sedimentary rocks for Units I and II in Holes 788A, 788C, 788D, and 789A.

Description of Units

Unit I

Intervals: Core 126-788A-4H, Cores 126-788C-1H through -26H, and Cores 126-788D-1R through -4R at 55 cm
Age: Pliocene to Quaternary
Depth: 0–249 mbsf

Sediments and sedimentary rocks assigned to Unit I were recovered from Holes 788A, 788C, and 788D. Hole 788A recovered only a single core-catcher sample. Hole 788D cored the basal 26 m of Unit I and recovered the contact with Unit II. Only Hole 788C cored the entire unit; it provides the principal basis for the lithologic description that follows.

Unit I consists primarily of light olive gray (5Y 6/2), olive black (5Y 2/1), and grayish black (N2), pumiceous granule and pebble gravel (Fig. 7) that, over a transitional interval from 172 to 230 mbsf (Section 126-788C-18H-CC to Core 126-788C-25H), progressively lithified to a conglomerate of essentially identical composition with that of the gravel that immediately overlies it.

Table 2. Summary of sediment types and sedimentary structures at Site 788.

Subunit	Lithology	Sedimentary structures	Interval (mbsf)	Age	Occurrence
IA (Transitional)	Pumiceous sandy granule and pebble gravel locally interbedded with vitric sands and rare vitric silts. Mean sand:granule:pebble ratio is 24:30:45. Maximum clast size is 130 mm. Oxidized coatings on clasts in Cores 126-788C-1H to -7H. Mn-oxide coatings on clasts in Cores 126-788C-5H to -8H. Transition to conglomerate in Cores 126-788C-19H through -24H.	Gravel predominantly structureless; local normal grading may be drilling artifact. Rare grading of vitric sand to vitric silt within interbeds.	0–229.2	Quaternary to Pliocene	126–788A-4R, 126-788C-1H to -24H 126-788D-1R
IB	Pumiceous sandy pebble-granule conglomerate. Mean sand:granule:pebble ratio is 15:32:52. Maximum clast size is 45 cm.	Structureless.	229.2–249	Pliocene	126-788C-25H to -26H 126-788D-2R to -4R, 55 cm
IIA	Interbedded nannofossil-rich claystone, vitric sandstone, vitric silty claystone, and vitric siltstone.	Vitric sandstones grade upward into vitric clayey siltstone and vitric silty claystone. Moderate burrowing; *Chondrites* common. Parallel lamination present.	249–278.6	Pliocene	126-788C-28X 126-788D-4R, 55 cm, to -7R, 8 cm
IIB	Interbedded pumiceous conglomerate, vitric sandstone, vitric siltstone, and vitric silty claystone. Toward the base, sandstone, siltstone, and claystone are carbonate bearing or carbonate rich. Faulting and fracturing in Cores 126-788D-8R through -10R.	Parallel lamination, wavy lamination, and locally intense bioturbation.	278.6–374	Pliocene	126-788D-7R, 8 cm, to -16R

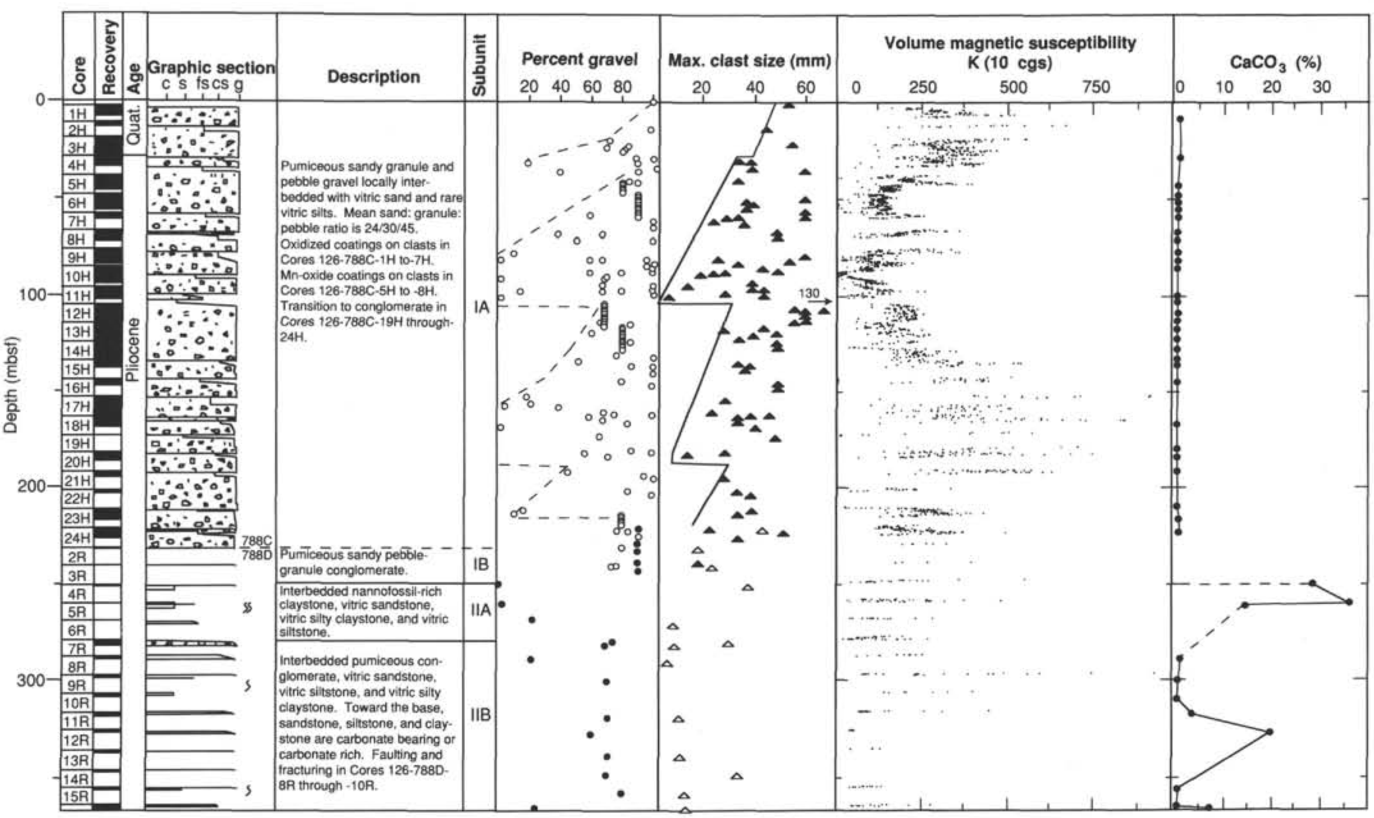

Figure 6. Lithostratigraphic summary diagram for Site 788, including a graphic display of core recovery, percent gravel, maximum clast size, and the downhole distributions of carbonate content and magnetic susceptibility. The carbonate curve is primarily a function of the distribution of nannofossil tests throughout the section, whereas the magnetic susceptibility data reflect the distribution of coarse mafic volcanic lithic rocks and crystals. The proportions of sediment types at Holes 788C and 788D are shown in the "Graphic section" column; the format is more generalized than in the core descriptions in that it reflects the percent of groups of lithotypes observed within any cored section (i.e., silt and clay, sand, gravel, carbonate), and does not show mixed biogenic/siliciclastic lithotypes. The graphic column is a simplified sedimentological log displaying relative grain size on the horizontal axis (c = clay/claystone, s = silt/siltstone, fs = fine-grained sand/sandstone, cs = coarse-grained sand/sandstone, and g = gravel/conglomerate); on this column, bedding within the core units is schematically displayed. Burrowed intervals are indicated to the right (see Fig. 6, "Explanatory Notes" chapter, this volume, for key to sedimentary structure symbols). The "Percent gravel" and "Maximum clast size" columns delineate four upward-coarsening cycles within Unit I, indicated by dashed and solid lines, respectively.

Table 3. Sediment recovery data for Units I and II at Site 788 and 789.

Subunit	Hole	Interval (core-core)	Depth (mbsf)	Cored (m)	Recovery (m)	Recovery (%)
IA	788A	1R	0			
		4R	45.3	45.3	1.24	3
	788B	1R	0			
		4R	35.6	35.6	0	0
	788C	1H	0			
		24H	229.2	229.2	[a]138.5	[a]60
	788D	1R	219.6			
		1R	229.2	9.6	0.79	8
	789A	1R	0			
		6R	54.1	54.1	0.10	0.2
IB	788C	25H	229.2			
		27H	249.0	19.8	0.63	3
	788D	2R	229.2			
		4R	249.0	19.8	0.94	5
IIA	788C	27X	249.0			
		28X	262.5	13.5	0.2	1.5
	788D	4R	249.0			
		7R	277.6	28.6	3.4	12
IIB	788D	7R	277.6			
		16R	374.0	96.4	7.2	7

Note: The Subunit IA/IB boundary is at the top of Core 126-788C-25H (229.2 mbsf) and the top of Core 126-788D-2R (229.2 mbsf). The Subunit IIA/IIB boundary is in Section 126-788D-7R-1 at 8 cm (277.58 mbsf, reported here as 277.6 mbsf).

[a] These figures are inflated by cave-in and flow-in at the tops and bottoms of cores, especially of vitric sand. The ODP coring summary reported a recovery of 8.78 m for Core 126-788C-19H, which contained large voids and actually contained only 1.94 m, the number used here.

This change in induration is the basis for dividing the unit into two subunits. The gravels and conglomerates of Unit I contain very little silt and clay and, consequently, very few microfossils.

Pumiceous, sandy, granule and pebble gravel constitutes 86% of Subunit IA. The sand/granule/pebble ratios in individual cores range from about 5/5/90 to 90/10/0; the mean ratio for the subunit is 24/30/45. The pumice is predominantly olive gray (5Y 4/1) to light olive gray (5Y 5/2) in color; however, from 0 to 58.2 mbsf (Cores 126-788C-1H through -6H), some pumice is oxidized to various shades of yellow, orange, and brown (10YR 6/8, 5/8, 7/4, 5/4; 5Y 7/2, 6/2). From 39.2 to 61.9 mbsf (Core 126-788C-5H to Section 126-788C-7H-CC), some of the pumice pebbles have thin (< 1 mm) surface coatings of olive black (5Y 2/1), brownish black (5YR 2/1), and grayish black (N2) manganese oxides (Fig. 8), some of which occur as microspherules (Fig. 9).

The dominant clast lithology in all of Unit I is pumice. Rhyolite pumice clasts are mostly aphyric, but some contain microlites (< 0.1 mm) of plagioclase and quench phases of clinopyroxene. With the exception of the interval from 48.8 to 97.0 mbsf (Cores 126-788C-6H, 14 cm, to 126-788C-11H-1, 58 cm), Unit I also contains clasts of glassy, commonly scoriaceous andesite in typical abundances of < 1%. These lithic clasts are significantly smaller than the associated pumice pebbles, ranging in intermediate diameters from 3 to 10 mm. Chemical data from the analysis of a clast of this andesite scoria are presented elsewhere (see "Igneous Geochemistry" section, this chapter). In smear slides, small amounts (< 2% total) of plagioclase, clinopyroxene, orthopyroxene, and oxide fragments are present in addition to the dominant glass shards. In the top of Core 126-788C-9H (78 mbsf), there are two clasts up to 6 cm in diameter of olive gray (5Y 3/2), vitric silty claystone, much more lithified than the sediments in this interval. Below about 135 mbsf (Core 126-788C-15H), clasts of mottled-green pumiceous breccia (Fig. 10) are also present.

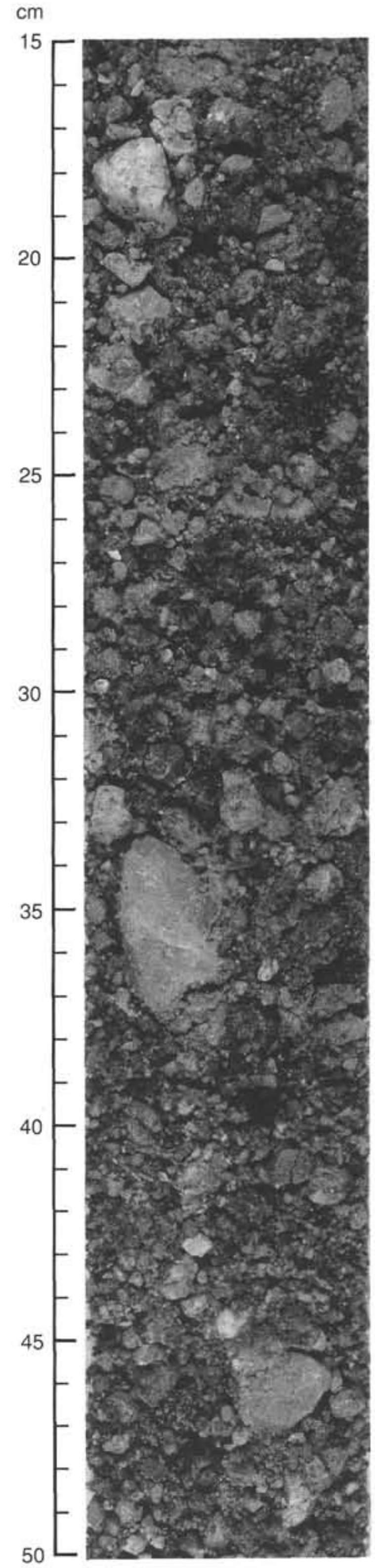

Figure 7. Pumiceous gravel in Subunit IA. The dominant color of the pumice is grayish black (N2); some clasts are yellowish brown (10YR 5/4). There are mixed basaltic and felsic clasts (Interval 126-788C-4H-3, 15-50 cm).

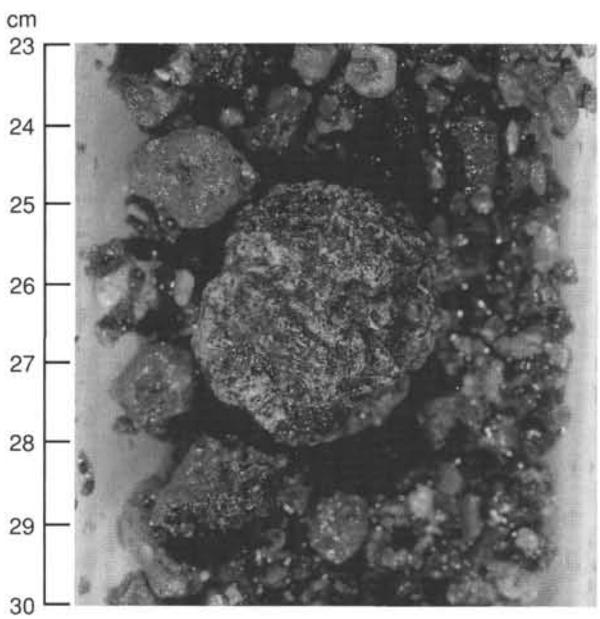

Figure 8. Pumice pebble with a black surface coating of manganese oxide (MnO_2). The diameter of the pebble is 3.5 cm (Interval 126-788C-5H-1, 23-30 cm).

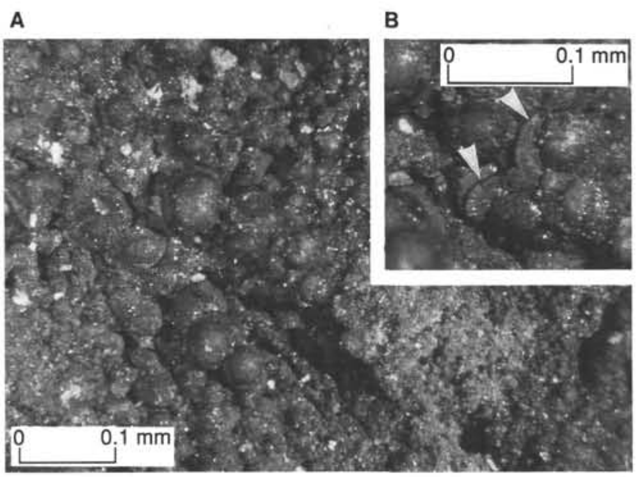

Figure 9. Microspherules of manganese oxide (todorokite) on the surface of a pumice pebble (Sample 126-788C-7H-CC, 20 cm). **A.** General view of the microspherules. Bar scales are 0.1 mm. **B.** Enlargement of an area just to the left of this inset, showing radial crystal habit of the todorokite where a microspherule has been broken open. Bar scales are 0.1 mm.

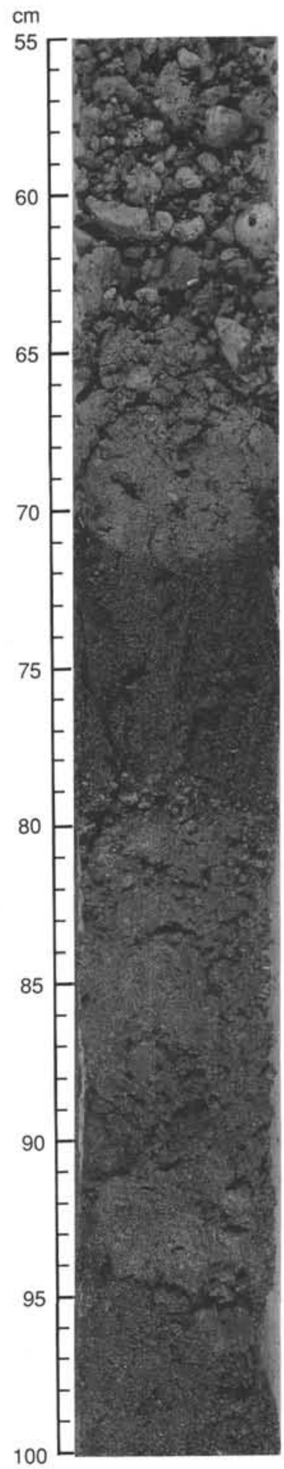

Figure 10. A light olive gray (5Y 6/1), fine vitric sand bed (64–70 cm) and a locally pebbly, dark gray (N4) vitric sand bed (70–79 cm) intercalated with well-sorted, pebbly granule gravel (Interval 126-788C-8H-2, 55–100 cm). Both sand beds are interpreted as ash layers.

The rest of Subunit IA is mainly structureless, silicic, vitric sand, much of which is present in disturbed intervals (cave-ins and flow-ins) at the tops and bottoms of cores; therefore, the relative abundance of this lithology (14%) within Subunit IA is overestimated in recovery figures (see Table 3). Minor, undisturbed sand beds within the cores (Fig. 11) are only 6–58 cm thick; two of these grade upward into 4- and 77-cm-thick intervals of vitric silt, the only appearances of this lithotype in the subunit. Beginning at 172 mbsf (Section 126-788C-18H-CC and Core 126-788C-19H), drilling biscuits of the semilithified gravel and conglomerate increase irregularly in abundance downhole (Fig. 12), with a corresponding decrease in the proportions of original unconsolidated gravel (or lithified material disaggregated by drilling). No cement was recognized, and induration is most likely a result of compaction.

The downhole trend in lithification is accompanied by a pronounced decrease in recovery to only 4% in Core 126-788C-

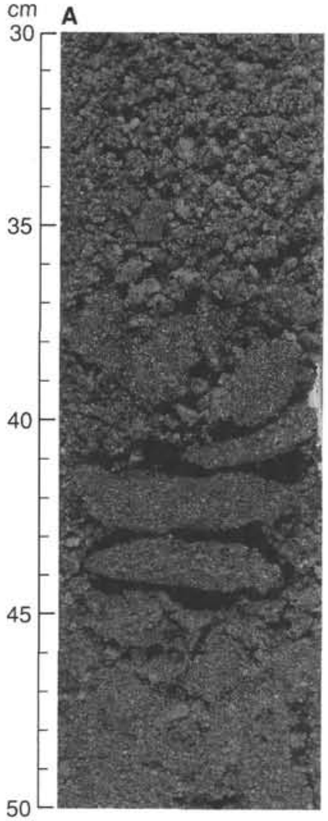

Figure 11. Transitional facies from granule gravel to granule conglomerate. **A.** In this example, the lithified fragments are "drilling biscuits" (40–44 cm) produced by coring. Above and below the lithified fragments, respectively, is granule gravel (sand 30%, granules 60%, pebbles 10%) and pumiceous medium sand (Interval 126-788C-20H-2, 30–50 cm). **B.** Lithified "biscuits" of pumiceous pebble conglomerate, surrounded by pumiceous gravel (sand 30%, granules 40%, pebbles 30%; Interval 126-788C-22H-1, 27–45 cm).

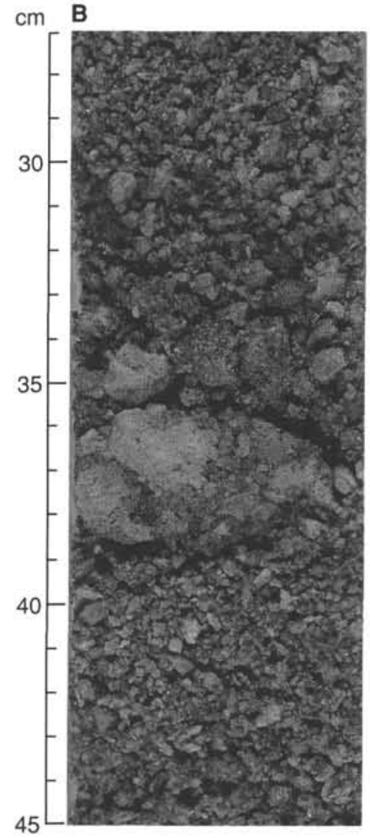

Figure 11 (continued).

25H, where the lithified clasts are as thick as 7 cm in diameter and more abundant than unconsolidated or disaggregated material, and so the contact with Subunit IB was placed here, at 229.2 mbsf (Fig. 13). Apart from its lithification, the conglomerate of Subunit IB is compositionally and texturally similar to the gravel of the lower part of Subunit IA, sand/granule/pebble ratios ranging from 10/30/60 to 60/30/10 in individual sections and averaging 15/33/52 for the subunit.

Core 126-788C-26H recovered only 0.28 m of rock, after which XCB coring began. Core 126-788C-27X recovered no material, so the contact of Units I and II, which may have occurred either in Core 126-788C-26H or -27X, was missed in Hole 788C. Core 126-788C-28X recovered a totally different lithology and was placed in Unit II (Fig. 13).

Unit II

Intervals: Core 126-788C-28X and Cores 126-788D-4R at 55 cm through -16R
Age: Pliocene
Depth: 249–374 mbsf

The first recovery of Unit II in Hole 788C (Core 126-788C-28X), 9 m below the contact recovered in Hole 788D, is a nannofossil-rich claystone that also shows a fraction of a percent of foraminifers on the split-core surface (Fig. 13). In Hole 788D, nannofossil-rich claystone occurs beneath drilling biscuits of Unit I conglomerate in Section 126-788D-4R-1. The uppermost claystone is 0.52 m below the top of this core, which is 248.5 mbsf, and so the contact between Units I and II is placed at 249 mbsf (Fig. 13).

The five sediment types delineated in Table 2 are based upon poor (8%) recovery. To qualify and organize these sparse data, Figure 14 presents the recovered thicknesses of each lithology and their depths of occurrence in the hole as a basis for lithostratigraphic reconstruction. The columns of sediment types are arranged by coarseness, which increases from left to right. Pumice conglomerate and vitric sandstone are the most abundant sediment types in Unit II (29% and 27% of total thickness recovered, respectively), followed by nannofossil-rich claystone (21%), vitric silty claystone (12%), and vitric siltstone (11%). Nannofossil-rich claystone is restricted to the upper portion of the unit, where no pumice conglomerates were recovered. These distributions are genetically significant and are the basis for dividing the unit into two subunits, IIA and IIB, at the base of the lowest nannofossil claystone, 277.6 mbsf (Section 126-788D-7R-1 at 8 cm).

Figure 14 provides some sense of how thinly intercalated the various lithotypes in Subunit IIA are. Nannofossil-rich claystone layers from 8 to 54 cm thick constitute 62% of the subunit. These rocks are slightly to heavily bioturbated (Fig. 15). Trace fossils include *Chondrites*. Carbonate contents average 18%; one sample (126-788D-4R-1, 107–109 cm) was calcareous enough (36.14%) to be termed a nannofossil claystone. Foraminifer and nannofossil tests are clearly visible but are poorly preserved. Much of the interstitial carbonate is micrite. Small amounts of glauconite contribute to the grayish green (5GY 6/1) and dark greenish gray (10Y 5/1, 4/1) colors of these rocks.

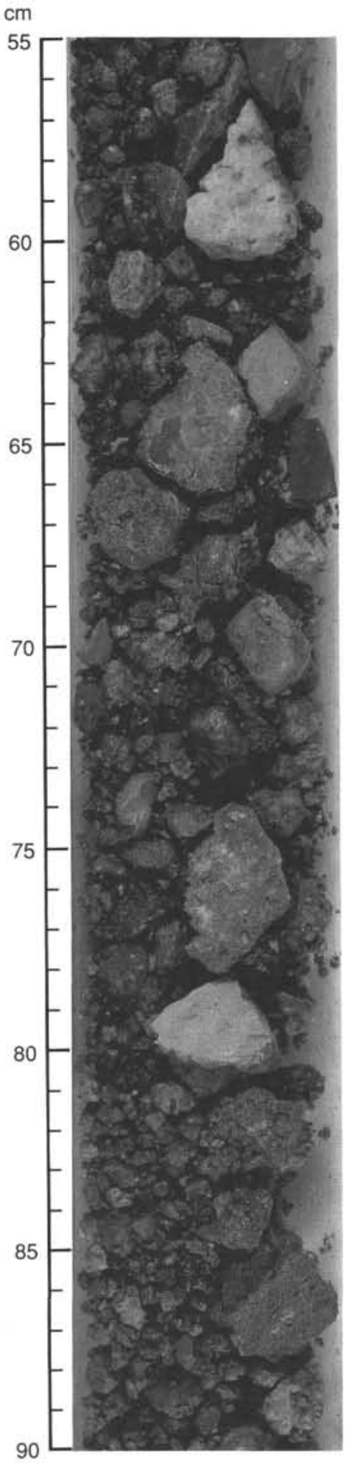

Figure 12. A diverse assemblage of lithic and pumice clasts in pumiceous gravel. The diameter of the lithic clast at 62–65 cm is 4 cm. The dominant color of the pumice gravel is olive black (5Y 2/1; Interval 126-788C-15H-3, 55–90 cm).

The nannofossil-rich claystone is interbedded with black (N1), very fine- to medium-grained vitric sandstone layers, 1–40 cm thick, that constitute 18% of Subunit IIA. Brown volcanic glass is the principal constituent of the sandstones. The thicker beds are planar laminated, and graded beds are succeeded by very dark greenish gray (10Y 3/1), clayey vitric siltstone, which comprises 8% of the subunit. The remaining 12% of the subunit consists of dark greenish gray (10Y 5/2) and greenish black (5GY 2/1), bioturbated mixtures of interbedded vitric sandstones and nannofossil claystones.

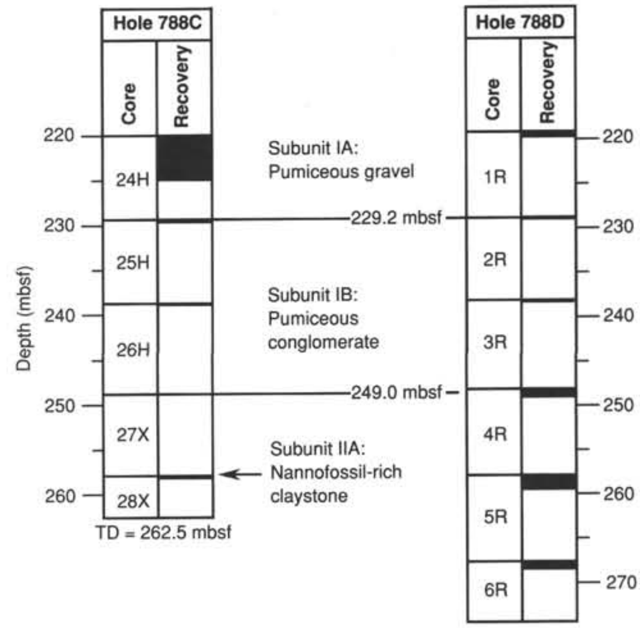

Figure 13. The basis for establishing the Subunit IA/IB and Unit I/II contacts at Site 788.

Subunit IIB is composed of pumiceous conglomerate (44%), vitric sandstone (30%), vitric siltstone (12%), and vitric silty claystone (9%). The conglomerate is grayish black (N2) and brownish black (5YR 2/1; Fig. 16). It is more poorly sorted than the gravel and conglomerate of Unit I and contains more sand (20%–40% vs. an average of 15%). Typical granule and pebble contents are 60%–80%, and maximum clast sizes are about 10 mm. Clasts are colored light olive gray (5Y 6/2), olive black (5Y 2/1), and grayish black (N2).

The vitric sandstone is grayish black (N2), medium to very fine grained, and is present in layers 5–36 cm thick (Fig. 17). Planar lamination is common, and one bed displays wavy laminations at its base. Vitric siltstone layers are 4–37 cm thick, grayish black (N2), and planar laminated, or they are light olive gray (5Y 6/2) or medium dark gray (N4) and either structureless or bioturbated (Fig. 18). Vitric silty claystone occurs as two laminated layers: one dark gray (5GY 4/1) and 60 cm thick (Core 126-788D-9R), the other greenish black (5G 2/1) and only 5 cm thick (Core 126-788D-13R, 0–5 cm).

Although Subunit IIB is generally characterized by the coarseness of its material and the scarcity of carbonate, it tends to become more calcareous in its middle portions and toward the bottom of the hole (Fig. 6). The enrichment in carbonate affects all lithotypes; conglomerate in Core 126-788D-12R, where nannofossils and foraminifers are part of the matrix, and vitric siltstone and silty claystone in Cores 126-788D-15R and -16R.

The rocks of Subunit IIB have been deformed by faulting (288–297 mbsf). In Section 126-788D-8R-CC, hanging-wall vitric sandstone has been juxtaposed against pebble-granule conglomerate along a healed, 7-mm-wide, siltstone-filled microfault zone that dips at 60° (Fig. 19). Another healed microfault dipping at 30° is located at the top of Core 126-788D-9R; here, granule conglomerate is the hanging-wall lithology, resting on vitric silty claystone with laminae that dip at 5° in the same direction as the fault. A total of six subvertical microfractures occur lower in the same core and in the next (Core 126-788D-10R),

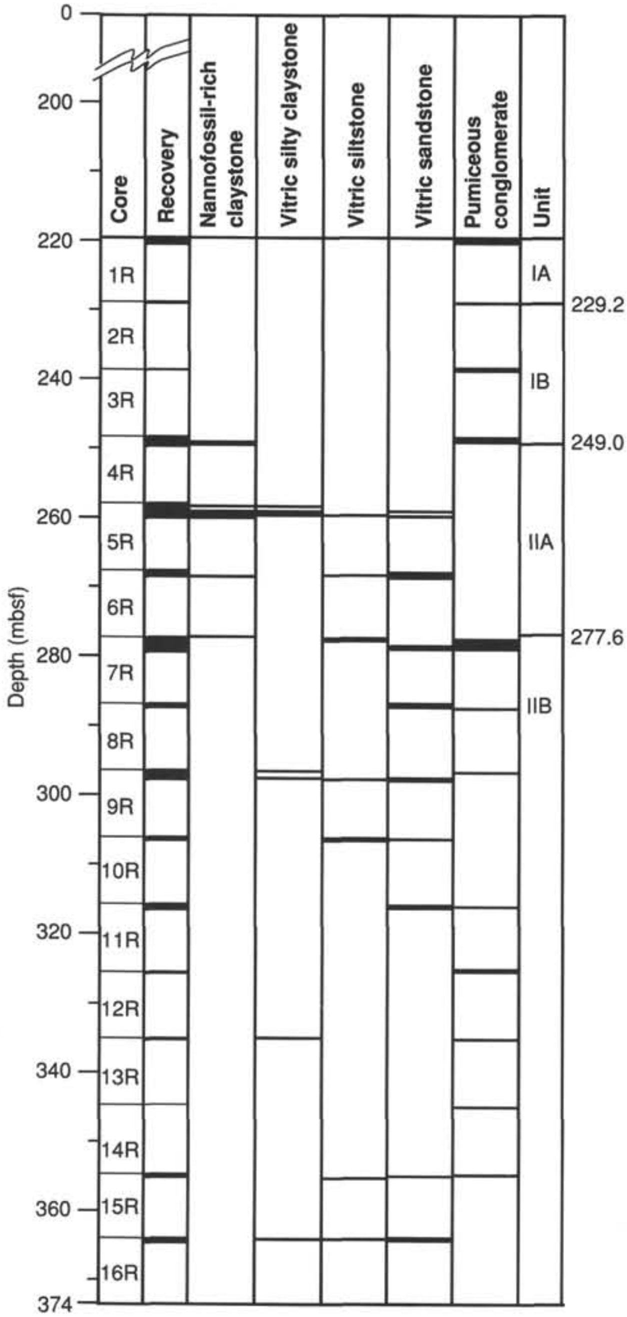

Figure 14. The lithotypes of Hole 788D, and the bases for defining the Unit I/II and Subunit IIA/IIB boundaries.

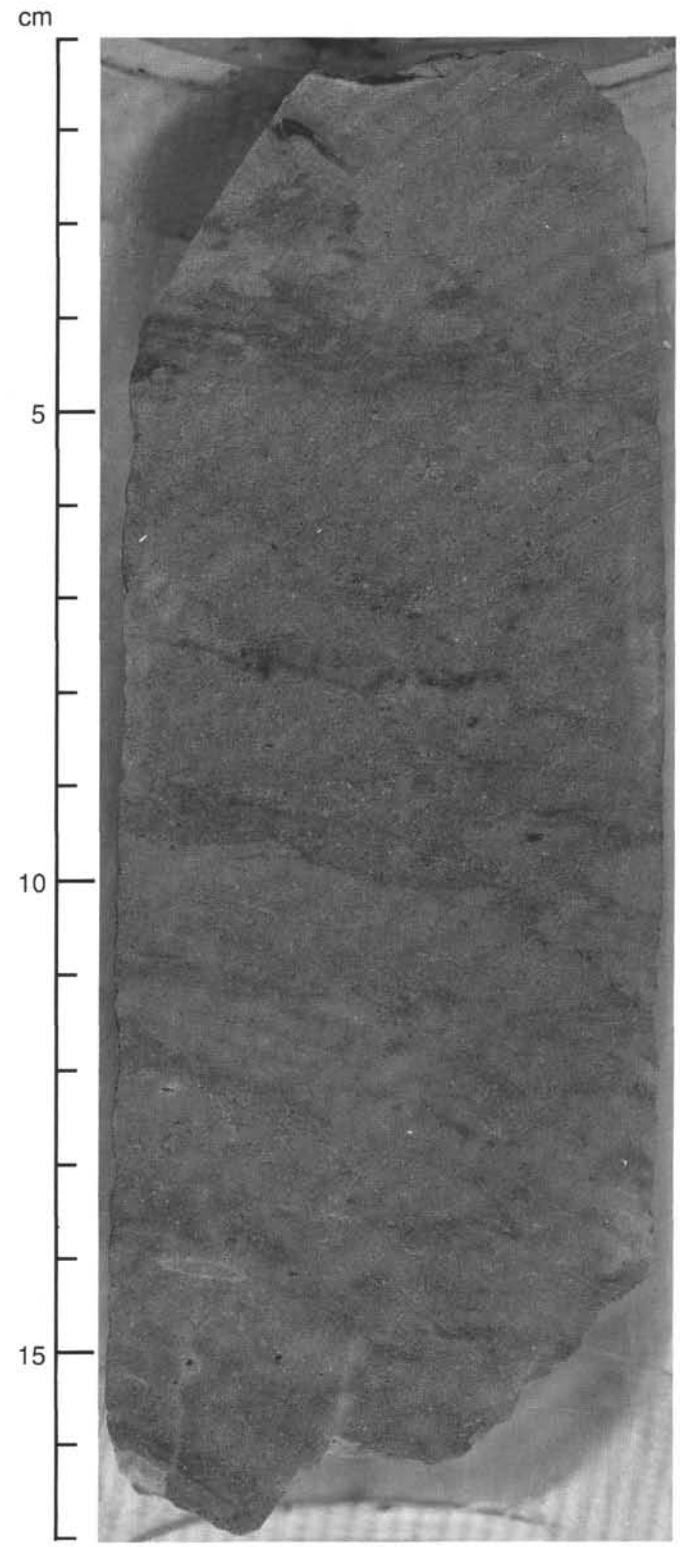

Figure 15. Strongly burrowed nannofossil claystone of Unit IIA with scattered white foraminifers (Interval 126-788C-28X-CC, 0–17 cm).

below which no additional evidence of tectonic deformation was seen.

Lithification and Diagenesis

Because lithification and diagenetically influenced parameters, such as nannofossil content, have been used to define subunit boundaries, these processes warrant further discussion. Petrographic examination of thin sections from Subunits IA (IA to IIB transition; Sample 126-788D-1R-1, 25 cm), IIA (Sample 126-788D-6R-1, 41 cm), and IIB (Samples 126-788D-9R-1, 89 cm; 126-788D-11R-1, 12 cm; and 126-788D-12R-1, 11 cm) show a downhole variation in lithification processes. Compaction and pressure welding are prevalent at the base of Subunit IA and in

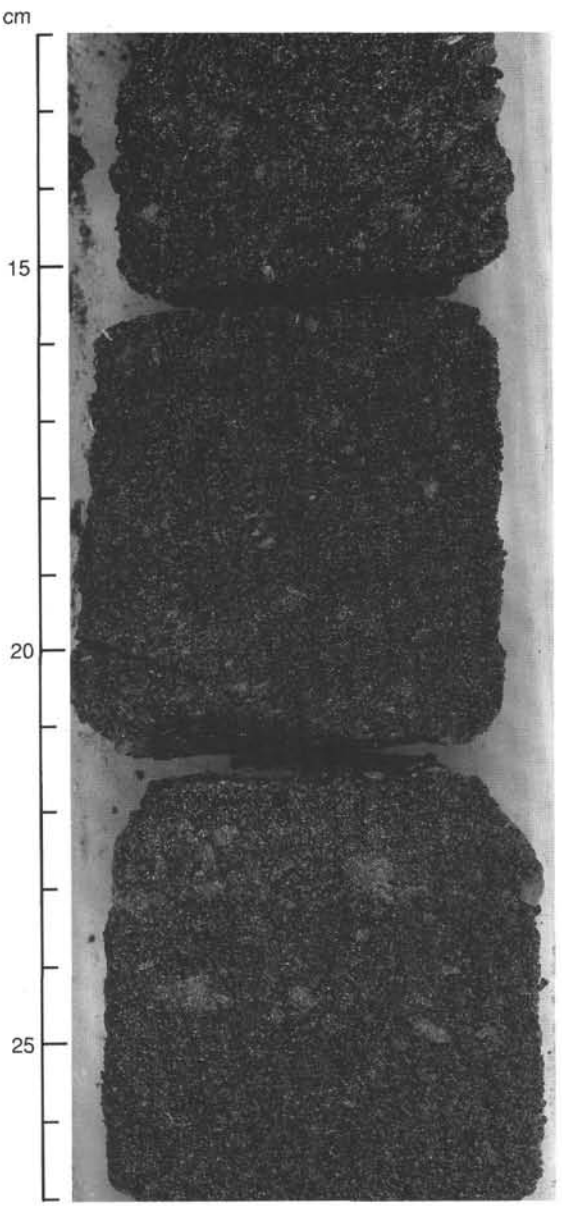

Figure 16. Black (N2), pebble-granule conglomerate characteristic of Subunit IIB (sand 30%, granules 40%, pebbles 30%; Interval 126-788D-7R-2, 12–27 cm).

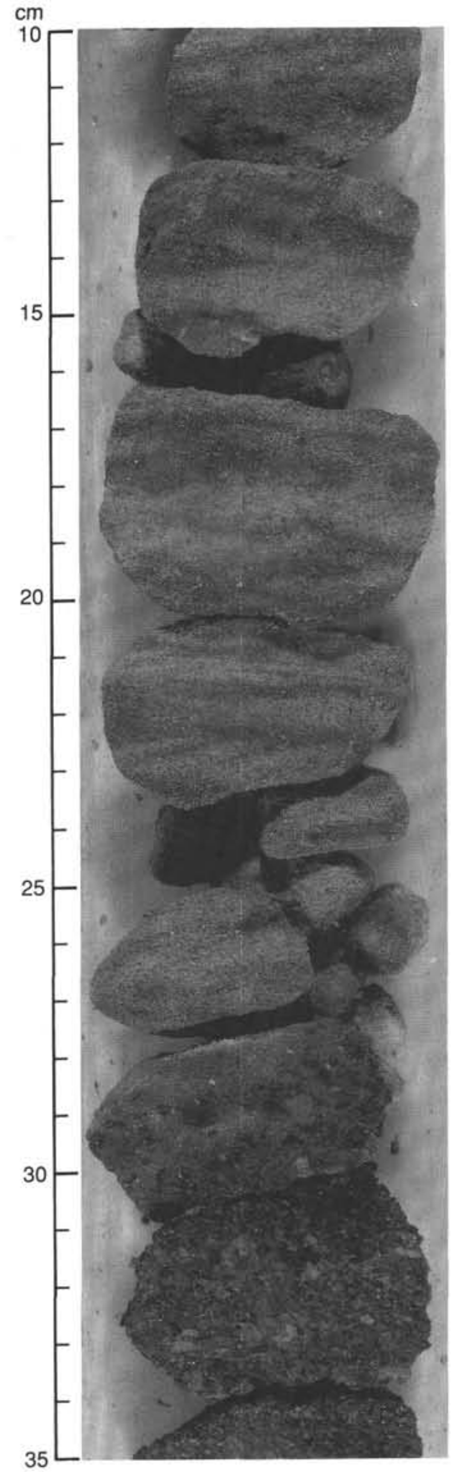

Figure 17. Pumiceous medium-grained sandstone (above 28 cm) and vitric sandy granule-pebble conglomerate (below 28 cm; Interval 126-788D-11R-1, 10–35 cm).

Subunit IIA, whereas compactional textures are accompanied by cementation in Subunit IIB. Smear-slide description of Sample 126-788C-21H-1, 2 cm, indicates that recrystallization of clay-mineral matrix material may also be an important binding agent in these sediments.

The uppermost occurrence of carbonate cement (high-Mg calcite; see XRD data) in Subunit IIB coincides with a shift in the preservation of calcareous fauna: Subunit IIA is nannofossil-rich, in direct contrast with Subunit IIB, which is relatively devoid of nannofossils but is locally enriched in foraminifers. Carbonate cements in Subunit IIB samples exhibit needle to microspar morphologies and also form needle overgrowths on foraminifer tests. Only one sample showed two-phase cementation: initial precipitation of carbonate needles, followed by precipitation of microcrystalline, low-birefringent zeolite. The paragenetic sequence is documented by the inclusion of carbonate crystals within the later zeolite phase. This local zeolite cementation could be related to glass hydration reactions within adjacent sediments.

Constituent grains of different morphologies and mineralogy have responded to compaction in different ways during induration. Where compactional processes have resulted in induration,

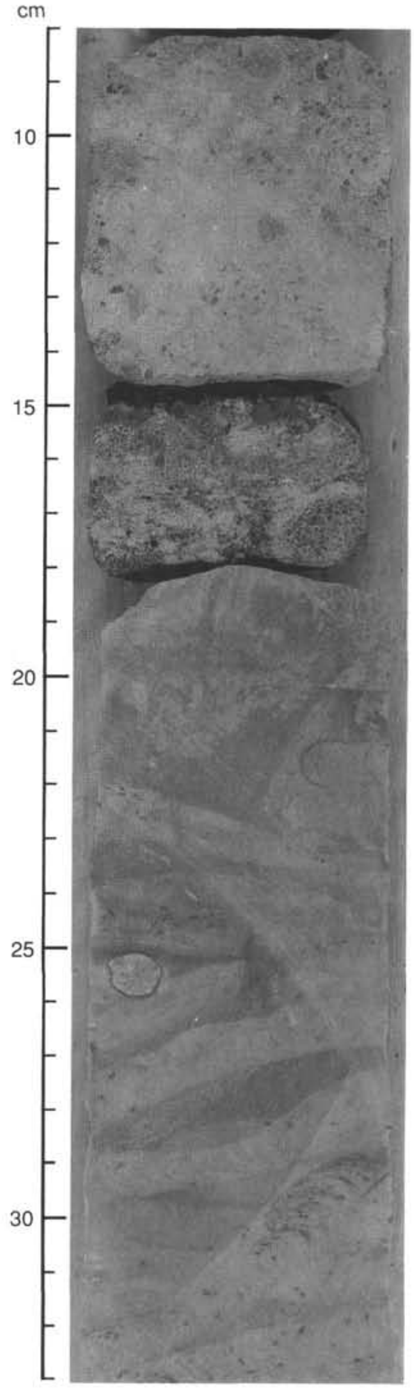

Figure 18. Strongly burrowed vitric siltstone in Subunit IIB. *Zoophycos* is the predominant trace fossil from 23-33 cm (Interval 126-788D-16R-1, 8-33 cm).

grain contacts are straight and interpenetrating, and deformed grains are common. Microporous pumice fragments, the most common grain type within Site 788 sandstones, are less competent than interspersed or interlaminated, altered microlitic to holocrystalline intermediate glass fragments. The glass fragments are embedded therefore into (interpenetrated) pumice grains or deform pumice grains at pressure-welded grain contacts. This pressure welding, caused by simple compactional processes within a pumiceous sequence, mimics high-temperature welding effects.

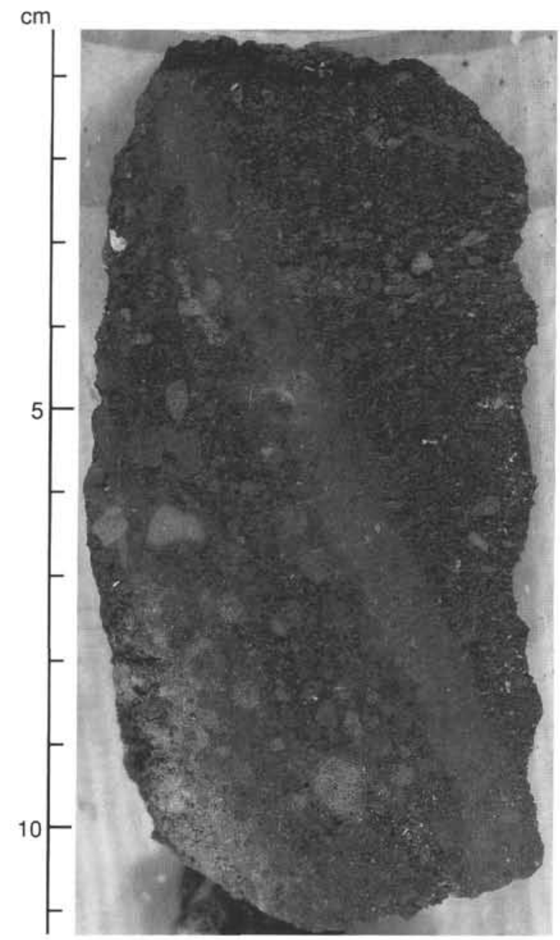

Figure 19. Fault in Subunit IIB. The fault dips at 60° and separates granule-bearing, fine-grained vitric sandstone (hanging wall) from mafic vitric sandy pebble-granule conglomerate (foot wall). A 5-mm-thick band of vitric silt fills in the fault (Sample 126-788D-8R-CC, 1-11 cm).

Brittle deformation is also observed within these sediments. Pumice grains and foraminifer tests are commonly fractured, shattered, or totally crushed as a result of compaction. Grain orientation and shape appear to play an important role in determining whether ductile or brittle deformation will occur. Chemical dissolution may also be important in foraminifer-rich, pumiceous sands, in which the foraminifers appear to be "pressolved" (dissolved as a result of pressure) along grain contacts. Within foraminifer-rich sandstones, the carbonate cements are localized around crushed foraminifers; thus, liberated carbonate may have been locally reprecipitated as microcrystalline cement.

X-Ray Diffraction Analysis

X-ray diffraction (XRD) results are summarized in Table 4. In Unit I, handpicked black microspherules (Fig. 9) on the surface of a pebble of pumice (Sample 126-788C-7H-CC, 20 cm) display a very strong peak at 0.95 nm, reflecting abundant todorokite $(Ca,K,Na)_{0.21}(Mn^{2+},Mg^{2+},Mn^{4+})_{6.40}O_{12} \cdot 3.6H_2O$ as well as large amounts of amorphous glass (Fig. 20). The black, manganiferous material coats the surface of pumice pebbles and granules from 38 to 78 mbsf (Cores 126-788C-4H to -9H). Buserite is not present in the microspherules. The todorokite is stable and did not change to birnessite after 15 days of air drying.

In the top of Subunit IIA, micrite-rich claystone contains glauconite, in association with smectite, calcite, and feldspar

Table 4. X-ray diffraction data from Site 788.

Core, section, interval (cm)	Depth (mbsf)	Unit	Color	Texture	Clay minerals: 1.4-nm	Clay minerals: 1.0-nm Mica	0.7-nm Chlorite	Minerals	1.0–1.1 nm 0.44-nm Palagonite	Amorphous materials
126-788C-										
7H-CC, 20	61.7	I	5YR2/1	Mn spherule	—	—	—	Todorokite >>> halite	—	Abundant
8H-3, 10	70.8	I	5Y4/1	Granular sand	—	—	—	Feldspar, halite	Common	Abundant
13H-1, 50	115.7	I	5GY3/2	Welded tuff	1.41-nm chlorite	Present	Abundant	Quartz, feldspar > halite	Present	Abundant
28X-CC, 15	257.9	II	5GY6/1	Micrite-rich claystone	1.76-nm mica-smectite interstratified	0.45-nm glauconite	Trace	Calcite > feldspar > quartz, halite	Common	Abundant
126-788D-										
1R-1, 50	220.1	II	5GY4/1	Conglomerate	Present	Present	Present	Feldspar >>> quartz, halite	Present	Common
6R-1, 20	268.1	II	5G4/1	Siltstone	1.76-nm smectite	Trace	Abundant	Feldspar >>> quartz > halite	—	Common
6R-1, 30	268.2	II	N1	Mafic vitric sandstone	1.76-nm smectite	—	—	Feldspar >>> halite	Common	Abundant
6R-1, 50	268.5	II	5Y2/1	Mafic vitric sandstone	Present	—	—	Feldspar	Present	Abundant
6R-1, 70	268.6	II	10Y4/1	Claystone	Present	—	Trace	Feldspar >>> calcite	Present	Abundant
11R-1, 13	316.1	II	5Y5/4	Pumiceous sandstone	Present	—	Trace	Calcite (Mg-rich) > feldspar > halite	Trace	Abundant

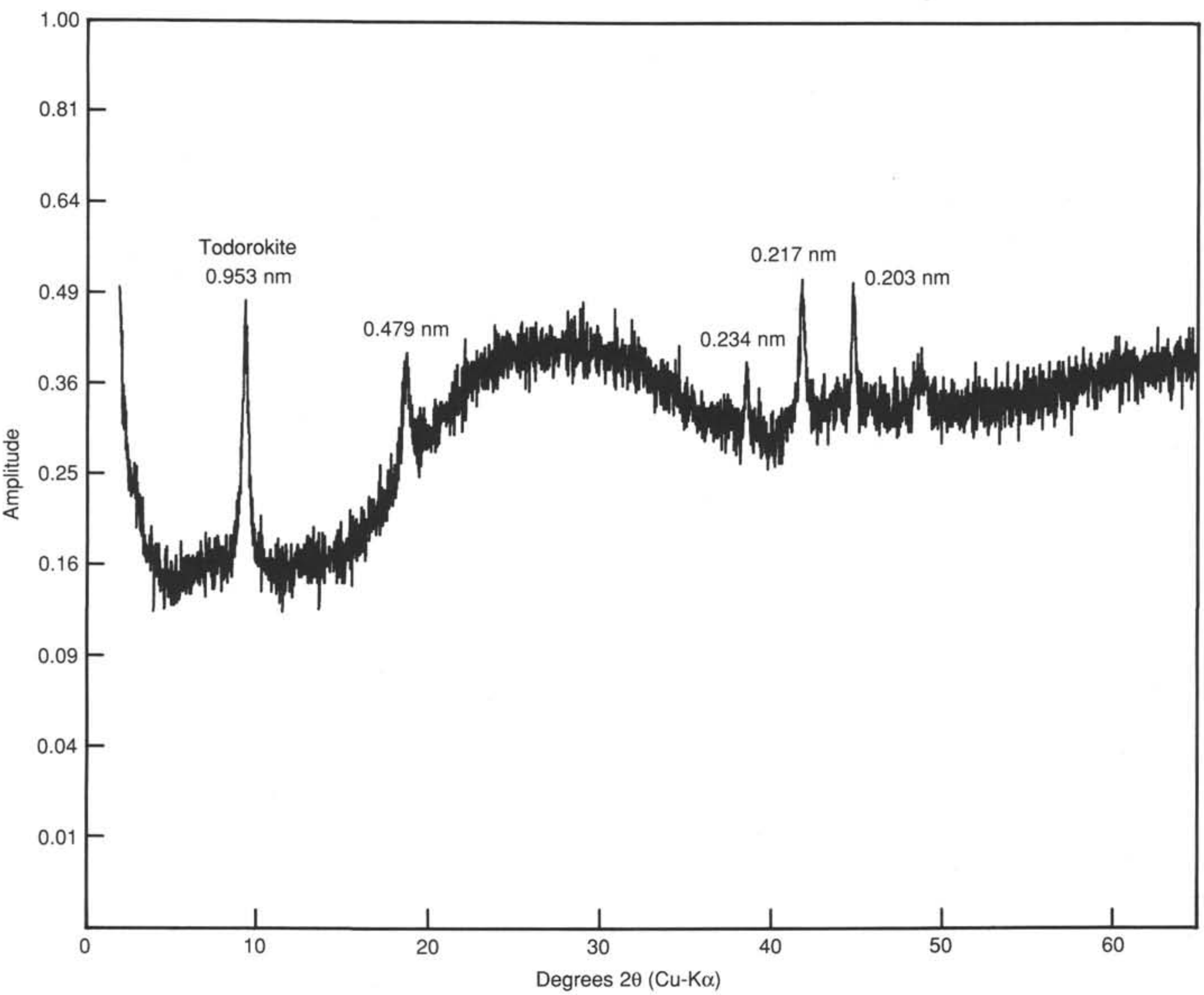

Figure 20. XRD pattern for handpicked spherules of manganese oxide, indicating the characteristic peak of todorokite (Sample 126-788C-7H-CC, 20 cm).

(Fig. 21). The sediment contains foraminifers and interstratified mica-smectite clay minerals. Glauconite is commonly confused with celadonite, an iron-rich, dioctahedral mica with almost the same chemical composition as glauconite. The Site 788 material shows a distinctive glauconite <060> reflection at a *d*-spacing of 0.151–0.152 nm that is larger than the analogous *d*-spacing of celadonite at 0.150 nm. This distinction of glauconite from celadonite is important, because celadonite is an alteration product or hydrothermal mineral associated with volcanic rocks. In contrast, glauconite indicates *in-situ* sediment alteration under reducing conditions with fairly slow sedimentation rates (Berner, 1981; Odin and Matter, 1981).

Green to black vitric siltstone and sandstone beds in Units I and II contain large amounts of amorphous material, principally volcanic glass. The glass, which is green to brown in color, is partially altered to smectite, chlorite, and palagonite. Feldspar is abundant in the vitric siltstones and sandstones, whereas mica group minerals and quartz are very rare.

A sample of pumiceous medium-grained sandstone (Sample 126-788D-11R-1, 1–13 cm) has a peak at 0.300 nm, suggesting the presence of Mg-calcite rather than calcite; calcite has its characteristic <104> peak at 0.3035 nm.

Sediment Accumulation Rates

Sedimentation rates for Site 788 were determined from calcareous nannofossils datums, nannofossil biozones, and paleomagnetic events (Table 5), which were used to construct the age-depth curves shown in Figures 22 and 23. Sedimentation rates were not determined for Site 789 because of the lack of recovery at this site.

Sedimentation rates for Unit II at Site 788 average 124 m/m.y. over the interval from 4.77 to 3.88 Ma (Fig. 22). However, Figure 23 (an expanded version of the lower sedimentary section of Site 788) shows that sedimentation rates during this interval are quite variable, ranging from 39 m/m.y. to as much as 282 m/m.y. The lowest rates occur at the top of Subunit IIA, the nannofossil-rich claystone interval, and coincide with other lithologic indicators (see "Interpretation" section that follows) of reduced sediment accumulation at this time.

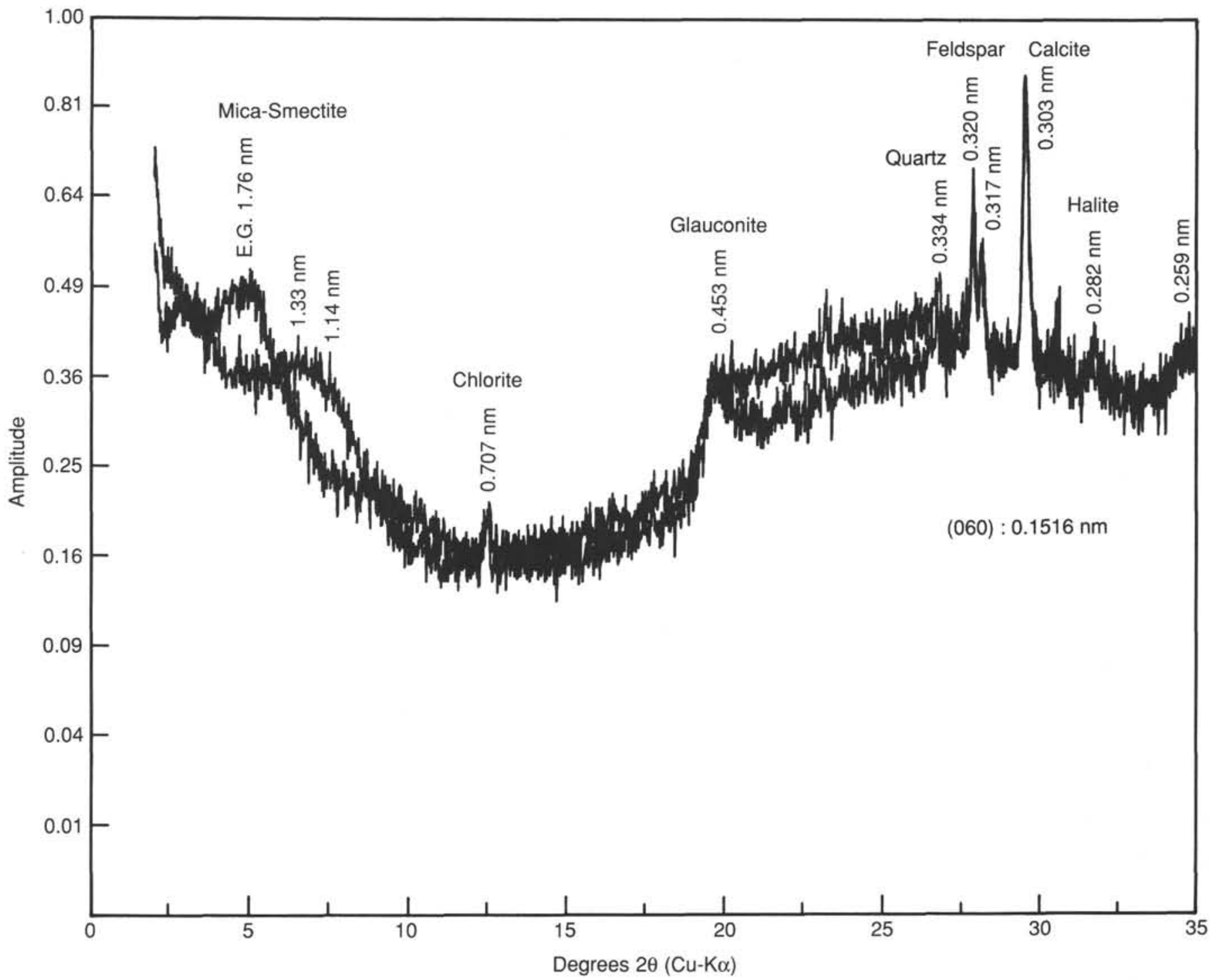

Figure 21. XRD pattern for micrite-rich claystone (Sample 126-788C-28X-CC, 15 cm) showing glauconite with mica-smectite interlayers, quartz, feldspar, and calcite.

Table 5. Chronostratigraphic events at Site 788 and associated depth intervals used to construct the age-depth curves shown in Figures 22 and 23.

Chronostratigraphic event	Core, section, interval (cm)	Depth (mbsf)	Age (Ma)
Biostratigraphy:			
FO. *E. huxleyi*	788A-4R-CC	27.43-35.80	<0.275
LO. *D. pentaradiatus*	788C-4H-1, 0-1	29.70-33.73	>2.350
Presence *Geophrocapsa* sp.	788C-19H-CC	180.98-181.78	<3.560
Paleomagnetics:			
Gilbert R to N	788D-4R, 85	249.35-257.90	3.88
N to R	788D-4R/5R	249.65-266.00	3.97
R to N	788D-5R, 15	258.35-266.15	4.10
N to R	788D-9R	297.00-306.50	4.24
R to N	788D-10R/11R	306.87-324.83	4.40
N to R	788D-11R, 55	316.55-325.38	4.47
R to N	788D-11R/12R	316.77-334.87	4.57
N to R	788D-15R/16R	355.28-373.28	4.77

Note: A slash ("/") between core numbers indicates that the polarity reversal occurred between the two cores listed. The two values for each depth datum represent the possible depth range a sample may have if less than 100% recovery occurred within a core. R = reversed polarity sequence and N = normal polarity sequence.

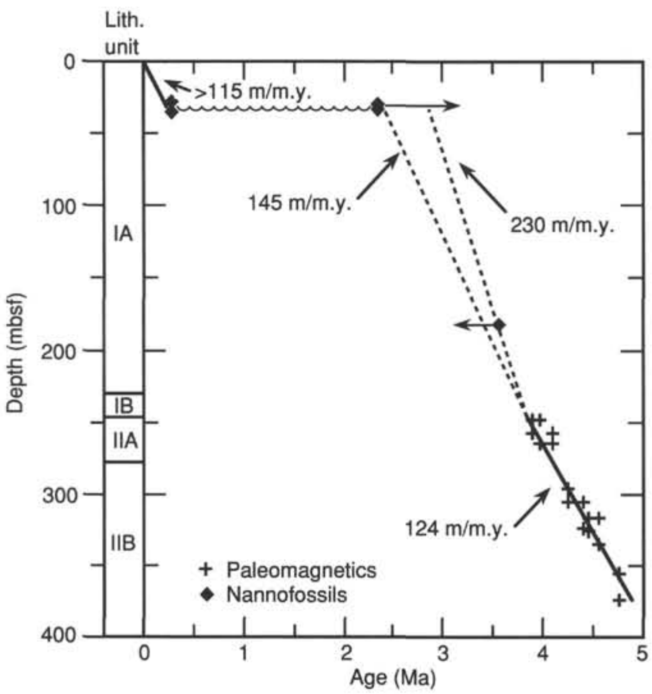

Figure 22. Age-depth curve for Site 788. See text and Table 5 for details of the chronostratigraphic horizons. Two points at any given event (age) indicate the possible depth range over which the event may have occurred.

Sedimentation rates in Unit I, the pumiceous sandy granule and pebble gravels, are constrained by nannofossil datums and biozones to vary between 145 to 230 m/m.y. for the interval between 30 and 250 mbsf (>2.35 Ma but <3.56 Ma). A hiatus, over 2.0 m.y. in duration, is present in the upper Pliocene to upper Quaternary sequence (2.35–0.275 Ma). Upper Quaternary (<0.275 Ma) sedimentation rates are no less than 115 m/m.y.

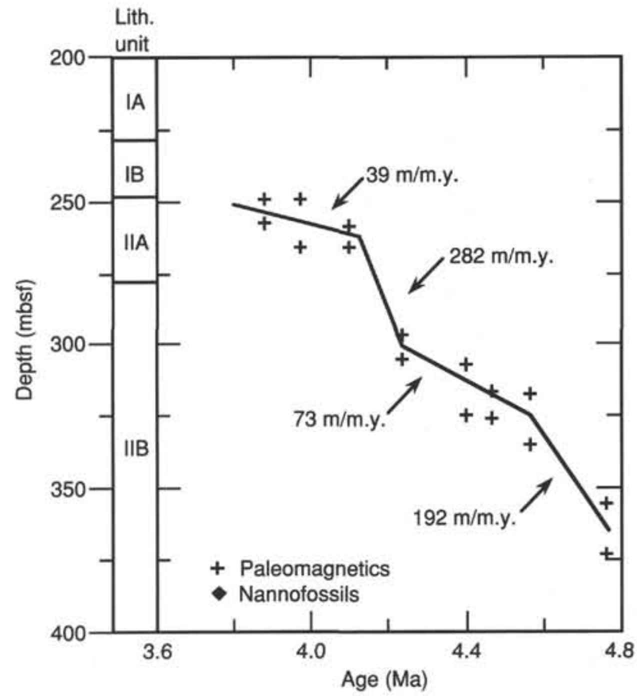

Figure 23. Age-depth curve for Site 788 for the interval from 250 to 370 mbsf. See Table 5 for details of chronostratigraphic horizons. Two points at any given event (age) indicate the possible depth range over which the event may have occurred.

and may be equivalent to rates in the pumiceous gravel below the hiatus.

Interpretation

Any attempt to reconstruct the history of Site 788 (Table 6) must be qualified by the poor recovery from Hole 788D. However, these rocks are a varied suite of lithotypes from which paleoenvironmental information of tectonic as well as sedimentologic significance may be extracted, with the caveat that the proportions of the recovered rock types, particularly that of easily disaggregated pumice conglomerate, probably do not accurately reflect the true proportions.

We begin with the environments and events recorded by the sedimentary rocks recovered from the bottom of Hole 788D (Subunit IIB). Initially high sedimentation rates (Fig. 23) accompanied nearby volcanism at 4.8–4.6 Ma. The carbonate contents of 4.6–4.2-Ma rocks, in the form of foraminifers and nannofossils, suggest that they were deposited during a fairly quiescent stage of volcanism. Otherwise, they would have been diluted by volcaniclastic debris. The relative abundance of foraminifers with respect to nannofossils may indicate that the site was already a bathymetric high subjected to winnowing by bottom currents this early in its history.

The pumiceous conglomerate in the upper portion of Subunit IIB was produced by active rhyolitic volcanism and was deposited on Site 788 some time between 4.2 and 4.1 Ma (Figs. 22 and 23). The presence of pressure welding and brittle compactional effects in the rocks of this subunit suggest that a significantly greater thickness of pumice may have been deposited, subjecting the rocks to high overburden pressures. If this is so, the overlying rock column must have been subsequently truncated by erosion, because the thickness of the present column is insufficient to create such effects. Sufficient overlying rock and

Table 6. Summary of geological events as deduced from the sedimentary data in Holes 788C and 788D.

Sedimentary event	Time period (Ma)	Environmental setting
1. Accumulation of pelagic carbonate and detrital component of basal Subunit IIB	4.8–4.2	Nearby volcanism, then volcanic quiescence; site bathymetrically high?
2. Accumulation of Subunit IIB pumiceous conglomerate	4.2–4.1	Massive silicic eruptions
3. Accumulation of Subunit IIA nannofossil-rich clays and associated rock types; glauconite diagenesis/authigenesis	4.1–3.8	Proximal volcanic lull; distal volcanism provides thin ashfalls; site was a bathymetric high, but with less relief and at greater water depth than during Subunit IA time
4. Accumulation of major part of Unit I pumiceous conglomerates and gravels	3.8–2.35 or later	Massive silicic eruptions; deposition of the first three cycles of pumice (from 249 up to 39.2 mbsf); the first two of these mixed andesitic-rhyolitic events or eruptive periods
5. Erosional truncation (tectonically triggered?) of Unit I pumice deposits	Sometime during 2.35–0.275	Site bathymetrically high
6. Accumulation of Subunit I manganese oxides		
7. Deposition of uppermost Unit I pumice layer (35.1–0 mbsf) on the manganiferous interval	Post 0.275	Massive silicic eruption(s)
8. Oxidation and reworking of surface pumices; remobilization of manganese oxides	Post-uppermost pumice deposition to Present	Site bathymetrically high

overburden pressure may not have accumulated until the time that Subunit IA was deposited.

The restriction of carbonate cementation to the interval immediately below the Subunit IIA/IIB boundary could be explained in three ways:

1. Fault- or unconformity-related juxtaposition of young, incipiently compacted sediments on more deeply buried, cemented sediments. This fault or unconformity would have to be situated between Cores 126-788D-6R (compacted only) and -9R (cemented and compacted), and would best correspond to the faulting observed in the interval from 288 to 297 mbsf (Sections 126-788D-8H-CC and 126-788D-9H-1).
2. A change in depositional environment (e.g., shallowing) between Subunits IA and IIB. This could best be verified by foraminiferal paleoenvironmental analyses.
3. Burial-related recrystallization and dissolution of nannofossil tests and associated pressolving of foraminiferal tests with reprecipitation in the form of needle and microspar cements in porous sandstones.

There is evidence to support the first and third of these hypotheses.

Another period of quiescence and slow deposition from 4.1 to 3.8 Ma is recorded by the lack of pumiceous conglomerates and the dominance of nannofossil-rich claystones in the rocks of Subunit IIA. Regional, distal volcanic activity, as recorded by the presence of thin vitric sandstones in the subunit, may have continued during this period but at a reduced scale. The glauconite in the nannofossil-rich claystones indicates that the claystones accumulated slowly and resided at the surface long enough for the glauconite to form authigenetically or from the diagenesis of other clay minerals.

In the modern marine environment, the typical site for glauconite accumulation is a submarine high, under conditions of either slow deposition or nondeposition, and nonoxidizing microenvironments (Odin and Matter, 1981) such as the tests of foraminifers. Berner (1981) has characterized the depositional environment of glauconite as one in which organic matter and sulfides are scarce or absent, and all oxygen has already been consumed by aerobic bacteria. If Site 788 was a bathymetric high during the time Unit II was deposited, the presence of significant amounts of fine material in the calcareous portions of the unit may signify that local relief was significantly less than at present. The site may also have experienced weaker bottom currents and other winnowing agents during Unit II deposition than it did during Unit I deposition because it was at greater depths.

After this period of slow deposition, explosive silicic volcanism was renewed at about 3.8 Ma, producing the first pumiceous gravels of Unit I. Upward-coarsening trends in the deposits indicate four major episodes of pumice eruption in late Pliocene to Quaternary time, or four extended periods over which silicic volcanism built up to climaxes. Each deposit is 30–50 m thick. These are roughly as thick as the individual Quaternary pumice layers at Site 791 and substantially thicker than those at Site 790. Being on the rift-basin floor, Sites 790 and 791 would be expected to accumulate thicker deposits than such high-standing localities as Sites 788 and 789. The Unit I pumice deposits of Pliocene age at Site 788 were either produced by individual events of greater magnitude than those recorded in the Quaternary deposits of Sites 790 and 791, or they were deposited during extended cycles of eruption. The top of the third upward-coarsening trend (29.7 mbsf; Interval 126-788-C-4H-1, 0–1 cm) is marked by an unconformity. The last of these accumulations is Quaternary in age, and thus is separated in time from the first three (see discussion below).

If the site stood above the surrounding submarine terrain during the accumulation of the Unit I pumice conglomerate and gravel, there are two plausible mechanisms that would have brought pumice clasts to the site and deposited them there as blankets. The pumice could have arrived more or less directly as air fall, or, alternatively, it may have rafted (or floated in the water column) to the site. That Subunit IA gravels are variably rounded, but very well-rounded pumice clasts in some intervals implies that they were subjected to extensive abrasion, perhaps from wave activity before or during their journey to the seafloor. This rounding supports the rafting transport mechanism rather than the direct air-fall one.

The occurrence of todorokite at depths of 39.2–61.9 mbsf is noteworthy. It addresses the question of whether hydrothermal activity has been significant at Site 788, and it bears upon the problem of locating a Pliocene hiatus at the site. Marine manganese oxides may be deposited (1) hydrothermally; (2) as a result of the slow oxidation of Mn^{2+} to Mn^{4+} during diagenesis; or (3) as hydrogenous precipitates from Mn-enriched seawater at the ocean floor. If manganese is derived from hydrothermal leaching of basalts in the basement, then the temperature range for this leaching would be in the 200°–500°C range.

Todorokite of Holocene hydrothermal origin has been found and studied in the Bonin region, in the vicinity of Nishinoshima Island, approximately 400 km south of Site 788. It is especially widespread on Kaikata Seamount. Usui et al. (1987) reported that the hydrothermal todorokite takes three forms, each characterized by its thickness and stability. Deposits thicker than 5 cm have stable, heat-resistant interiors, although their external portions may be unstable when heated at 110°C, as are deposits 1-5 cm thick, becoming transformed to birnessite. Deposits several millimeters to a centimeter thick are even less stable, becoming birnessite when air dried at room temperatures for 1 hr.

The todorokite in Subunit IA, although no more than a millimeter thick, remained unchanged after 15 days at room temperature, and probably has a different origin than the hydrothermal todorokites from the Nishinoshima area. A diagenetic or hydrogenous origin, on the other hand, would produce stable manganese minerals. The restriction of the manganese oxides to a relatively thin, near-surface interval far above the igneous basement is difficult to account for by hydrothermal origin *in situ*. Furthermore, the geochemistry of pore waters from Hole 788C (see "Sediment/Fluid Geochemistry" section, this chapter) is not very different from that of normal seawater. The manganese contents of these interstitial waters are only 30 ppm at depths of 135–215 mbsf, increase to 60 ppm at 60 mbsf, the lowest (and most abundant) occurrence of manganese, and then diminish to 50 ppm at 10 mbsf. It appears that the manganese in the pore waters is being remobilized out of the deposits. There is no other geochemical evidence for hydrothermal alteration of the sediment column or of its water content.

The manganese oxides occur close to an unconformity at approximately 30 mbsf (see "Biostratigraphy" section, this chapter). Nannofossil data established a Quaternary (<0.275 Ma) age for Section 126-788A-4R-CC at a depth between 27.5 and 35.8 mbsf. In Hole 788C, however, nannofossil data indicate a Pliocene age (≥2.35 Ma) at 29.7–33.7 mbsf (Sample 126-788C-4H-1, 0–1 cm, Table 5). These biostratigraphic data require that an unconformity exists at some depth between 27.5 and 33.7 mbsf. This is the cored interval of Cores 126-788C-3H to -4H. If the manganese in the depth range from 39.2 to 61.9 mbsf has a hydrogenous origin, it may mark a period of virtual nondeposition some time during the 2-m.y. hiatus. It remains to be demonstrated, however, that manganese could have precipitated on the pumice at some depth beneath, instead of directly on, the seafloor.

An explanation for the unconformity is that it was caused by rift-related Pliocene-Quaternary tectonism. As a result of tectonically triggered movements, a thick cap of gravel and other sediments that may have accumulated during all or part of the 2 m.y. of hiatus could have been removed by mass movements. This would account for the missing column of sediment necessary to provide the pressure to compact the conglomerates of Subunits IB and IIB. The compactional history of this sequence of sediments could be of great importance in estimating relative uplift rates during rifting in the Sumisu region. With the present limited data base, it is not possible to determine the amount of Pliocene-Pleistocene overburden that may have been removed by erosion during flank uplift.

The uppermost 30 m of pumiceous gravel atop the manganese at Hole 788C could have been deposited at any time after 2.35 Ma. Assuming that it correlates with the sequences of Hole 788A, it is 0.275 Ma in age or younger. Marked as the uppermost upward-coarsening sequence in Figure 6, this layer differs from the rest of the subunit in two ways. Many of its pumice pebbles are oxidized, and, although the entire subunit is depleted in fines, this uppermost layer is exceptionally so (Fig. 6). These features suggest that these surface deposits have resided for an extended period of time at the present seafloor atop this high-standing site, where the sediment is subjected to winnowing by currents and the slow oxidation of volcanic glass.

BIOSTRATIGRAPHY

Site 788

Calcareous Nannofossils

Hole 788A

Samples 126-788A-1R-CC, 126-788A-4R-1, 0–1 cm, and 126-788A-4R-CC contain *Emiliania huxleyi,* which falls within Zone CN15. Other species present in these samples are *Helicosphaera carteri, Gephyrocapsa* spp., *Pontosphaera* spp., *Reticulofenestra* sp., *Oolithotus antillarum,* and reworked specimens of *Pseudoemiliania lacunosa.*

Sample 126-788A-3R-CC is barren of calcareous nannofossils. Sample 126-788A-5R-CC contains only the species *P. lacunosa,* which has a range from the middle Pliocene to the Pleistocene (Zones CN11b–CN14a).

Hole 788B

No samples were taken or analyzed from this hole.

Hole 788C

Samples 126-788C-4H-1, 0–1 cm, 126-788C-4H-4, 30 cm, 126-788C-28X-1, 0–1 cm, and 126-788C-28X-CC contain species *Discoaster pentaradiatus, Discoaster brouweri,* and *Calcidiscus macintyrei* and do not contain *Discoaster surculus, Discoaster tamalis,* or *Reticulofenestra pseudoumbilica,* which suggests assignment to upper Pliocene Zone CN12c. Other species present in these samples are *Gephyrocapsa* spp., *Calcidiscus leptoporus, Coccolithus pelagicus, Helicosphaera sellii, Syracosphaera* sp., and small *Reticulofenestra* sp.

Samples 126-788C-4H-CC and 126-788C-19H-CC contain only rare specimens of *Gephyrocapsa* sp. The presence of *Gephyrocapsa* sp. in Sample 126-788C-28X-CC indicates that the bottom of this hole is no older than the middle Pliocene (Perch-Nielsen, 1985).

Preservation in these samples is generally poor to moderate because of dissolution of the calcareous nannofossils. This suggests that the absence of index species older than CN12c could be a result of dissolution. If so, the oldest constraint for the hole would then be based upon the first occurrence (FO) of *Discoaster pentaradiatus* in middle Miocene Zone CN7a (Perch-Nielsen, 1985).

All other samples taken from this hole are barren of calcareous nannofossils.

Hole 788D

Samples 126-788D-4R-CC, 126-788D-10R-1, 37 cm, 126-788D-12R-1, 28 cm, Core 126-788D-14R, and Sample 126-788D-16R-1, 12 cm, contain *Calcidiscus macintyrei,* which indicates an age range from the early Miocene to the early Pleistocene (Zones CN3–CN14a).

Sample 126-788D-5R-1, 10 cm, contains *C. macintyrei* and *Discoaster* sp. Therefore, it is no younger than the late Pliocene based on the last occurrence (LO) of the genus *Discoaster,* and no older than the early Miocene (Zone CN3) based on the FO of *C. macintyrei. Reticulofenestra* sp., *Gephyrocapsa* sp., and *C. leptoporus* are present in Samples 126-788D-6R-CC; 126-788D-11R-1, 18 cm; 126-788D-11R-CC; 126-788D-12R-CC; 126-788D-13R-1, 5 cm; and 126-788D-15R-1, 55 cm. All other samples analyzed from this hole are barren of calcareous nannofossils.

Planktonic Foraminifers

Hole 788C

Sample 126-788C-28X-CC, 5-6 cm, contains dextral *Globorotalia menardii,* dextral *Globorotalia tumida, G. crassaformis* s.l., *G. margaritae, G. scitula, Globigerinoides sacculifer, G. obliquus, G. bollii, Globoquadrina altispira, G. humerosa, G. venezuelana, Globigerina praedigitata,* and dextral *G. pachyderma.* The presence of *G. margaritae* and other assemblage species limits the age to Zones N18-N19 (Bolli et al., 1985).

Sample 126-788C-28X-CC, 13-14 cm, contains most species present in Sample 126-788C-28X-CC, 5-6 cm, plus *Globigerina ruber,* which makes its appearance in the middle of Zone N18 (Bolli et al., 1985). This sample is assigned to the middle of Zones N18-N19 according to the zonation of Berggren et al. (1985).

Sample 126-788C-28X-CC, 14-18 cm, contains, in addition to the species present in the previous sample, *Globorotalia merotumida-plesiotumida,* which ranges from the top of Zone N17 to lower Zone N19 (Bolli et al., 1985). This sample is assigned to middle Zone N18 to lower Zone N19.

Hole 788D

Sample 126-788D-4R-CC contains dextral *Globorotalia tumida,* dextral *G. menardii, Globigerinoides ruber, Globoquadrina altispira, G. humerosa, Orbulina universa,* and *Globigerina quinqueloba* placing this sample in the middle of Zones N18-N19 (Bolli et al., 1985).

Rare specimens of *Globorotalia margaritae,* in addition to *Globigerinoides conglobatus, G. humerosa, G. altispira, G. dutertrei,* dextral *Globigerina pachyderma,* and *Globorotalia crassaformis* s.l., were observed in Sample 126-788D-6R-CC, placing it in Zones N18-N19 (Bolli et al., 1985).

Samples 126-788D-15R-1, 38-40 cm, and 126-788D-16R-1, 37-39 cm, contain planktonic foraminifer shell fragments, which could not be identified at 100× magnification. The shells may belong to *Globoquadrina* sp., *Turborotalia* sp., *Globigerina* sp., and a menardiform-tumidaform species. They will be reexamined under the scanning electron microscope (SEM) during shore-based analyses for species identification.

Benthic Foraminifers

The benthic foraminifer fauna from Samples 126-788C-28X-CC, 5-6 cm, 126-788C-28X-CC, 13-14 cm, 126-788C-28X-CC, 14-18 cm, 126-788D-4R-CC, and 126-788D-6R-CC is characterized by an abundance of small, unornamented *Stilostomella* spp. Other common species are *Chilostomella* sp., *Pyrgo murrhina, Uvigerina hispida, Cassidulinoides* sp., *Pleurostomella* sp., and *Cibicidoides* sp. This fauna indicates a depositional water depth of 1500-3000 m (Ingle, 1980; Woodruff, 1985; Van Morkhoven et al., 1986; Yasuda, 1989). Abundant occurrences of anaerobic fauna (Bernhard, 1986) composed of small unornamented *Stilostomella* spp., *Chilostomella* sp., *Pleurostomella* sp., and a few occurrences of aerobic fauna from three samples from 126-788C-28X-CC indicate low- to medium-dissolved oxygen content. The fauna from the other samples have a higher ratio of aerobic fauna than the fauna from Sample 126-788C-28X-CC and show medium oxygen content.

Radiolarians

All samples analyzed from Holes 788A, 788B, 788C, and 788D were found to be barren of radiolarians.

Site 789

Hole 789A

Sample 126-789-1R-CC contains the calcareous nannofossil *Pseudoemiliania lacunosa,* which constrains the age of this sample from the early Pliocene to the Pleistocene (Zones CN11-CN14a of Okada and Bukry, 1980). Other nannofossil species present are small *Reticulofenestra* sp., *Calcidiscus leptoporus,* and *Helicosphaera carteri.*

No planktonic foraminifers, benthic foraminifers, or radiolarians were found at this site.

Summary

Calcareous nannofossils recovered from Hole 788A suggest a Quaternary age. Calcareous nannofossils suggest a middle to late Pliocene age for samples in Hole 788C. Planktonic foraminifers indicate an early to middle Pliocene age for Samples 126-788C-28X-CC, 5-6 cm, and 126-788C-28X-CC, 14-18 cm.

Most samples in Hole 788D were barren of calcareous nannofossils and planktonic foraminifers. Samples that did contain nannofossils show the effects of strong dissolution. However, planktonic foraminifers in Samples 126-788D-4R-CC and 126-788D-6R-CC restrict their age to the early Pliocene.

Benthic foraminifers indicate a depositional water depth between 1500 and 3000 m for Holes 788C and 788D. Most assemblages from these holes indicate a low to medium dissolved oxygen content.

PALEOMAGNETICS

Introduction

Magnetic measurements for Site 788 were confined to the cores with the finer-grained or more consolidated lithologies, because previous polarity assignments on coarse-grained, unconsolidated material drilled with the APC proved difficult because of the remanence acquired during drilling. Archive halves of all cores judged suitable for paleomagnetic study by this criteria, excluding cores composed of fragments too small to insure vertical orientation, were measured on the cryogenic magnetometer system.

In addition, a small number of discrete samples were demagnetized and measured on the fully automatic spinner (FAS) magnetometer (see "Explanatory Notes" chapter, this volume). These samples were taken from intervals of specific interest or where continuous core measurements were ambiguous. Alternating field (AF) demagnetizations at higher alternating fields in these cases provided a more confident picture of the characteristic polarity.

Magnetostratigraphy

Holes 788A and 788B

No magnetic results were obtained from these holes because of low core recovery.

Hole 788C

Based on lithology and degree of consolidation, only Core 126-788C-28X (257.9-262.5 mbsf) was judged suitable for polarity assignment The core exhibited a normal polarity after AF demagnetization to 8 mT. The lower to middle Pliocene fossil assemblage of this core (see "Biostratigraphy" section, this chapter) suggests that this normal polarity represents either the Gauss (indicated by the nannofossil assemblage) or Gilbert normal (indicated by the foraminiferal assemblage) polarity chron (Table 7).

Hole 788D

Cores 126-788D-4R through -16R (except Core 126-788D-14R, which has small fragments that may have rotated vertically) were all judged suitable for paleomagnetic measuring. Figure 24 summarizes the polarity designations, and Figure 25 shows the directional and intensity stability of several of the discrete samples measured from this hole. The increase in remanence intensity with AF demagnetization at 25 mT for Sample 126-788D-10R-1,

Table 7. Depth ranges for Gilbert and Gauss normal polarity chron datums.

Absolute age (Ma)		Depth range
Gilbert	Gauss	(mbsf)
3.88	2.47	249.35–257.90
3.97	—	249.65–258.2
4.10	—	258.35–266.15
4.24	2.92	297.0–298.32
4.40	2.99	306.87–316.0
4.47	3.08	316.55–325.38
4.57	3.18	316.77–325.6
4.77	3.40	355.28–364.3

30 cm, is characteristic of removal of the present-field normal overprint from a reversely magnetized sample.

The polarity sequence in Figure 24 may be correlated with either the Gilbert (#4) or Gauss (#3) normal polarity chrons. The compressed N-R polarity interval at the top of the section in the Gilbert correlation (Fig. 24A) would agree with the low sedimentation rate postulated for Cores 126-788D-4R and -5R, based on the presence of claystone and glauconite (see "Lithostratigraphy and Accumulation Rates" section, this chapter). The correlation with the older Gilbert normal chron requires that the reversely magnetized tuff bed (as measured in the continuous pass-through and the discrete sampling modes), which occurs in the upper 10 cm of Section 126-788D-5R-1, be representative of a full reverse polarity zone. The planktonic foraminifer assemblages of various cores from this hole have been associated with Zone N19 (see "Biostratigraphy" section, this chapter) and is consistent with the correlation to the Gilbert polarity chron.

Hole 789A

No magnetic results were obtained from this hole because of the limited recovery (0.10 m).

IGNEOUS GEOCHEMISTRY

Although the Pliocene-Pleistocene lavas hoped for at Site 788 did not materialize, there are white and black vitreous pumices in Subunit IA (see "Lithostratigraphy and Accumulation Rates" section, this chapter). Bulk chemical analyses of two of these, one rhyolitic, the other andesitic, are given in Table 8, together with seven analyses of Pleistocene rhyolite pumices from Sites 790, 791, and 792. For comparison, analyses are given for Quaternary acid andesite from the Izu-Bonin Arc (Tori Shima;

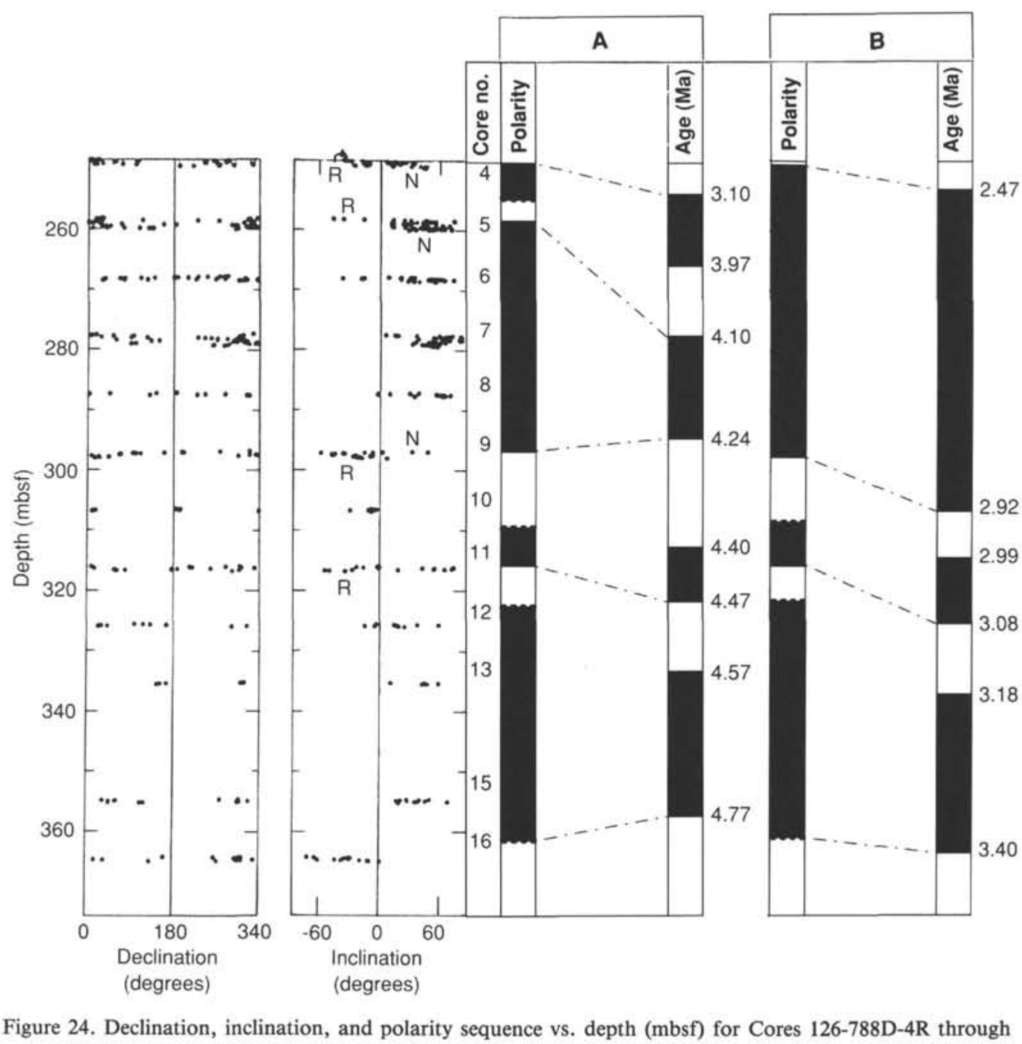

Figure 24. Declination, inclination, and polarity sequence vs. depth (mbsf) for Cores 126-788D-4R through -16R after demagnetization. Rough edges on boundaries indicate polarity transitions that occur between core sections. Datums and polarity sequence at the far right of each section are for the **(A)** Gilbert (#4) and **(B)** Gauss (#3) normal polarity chrons (Berggren et al., 1985).

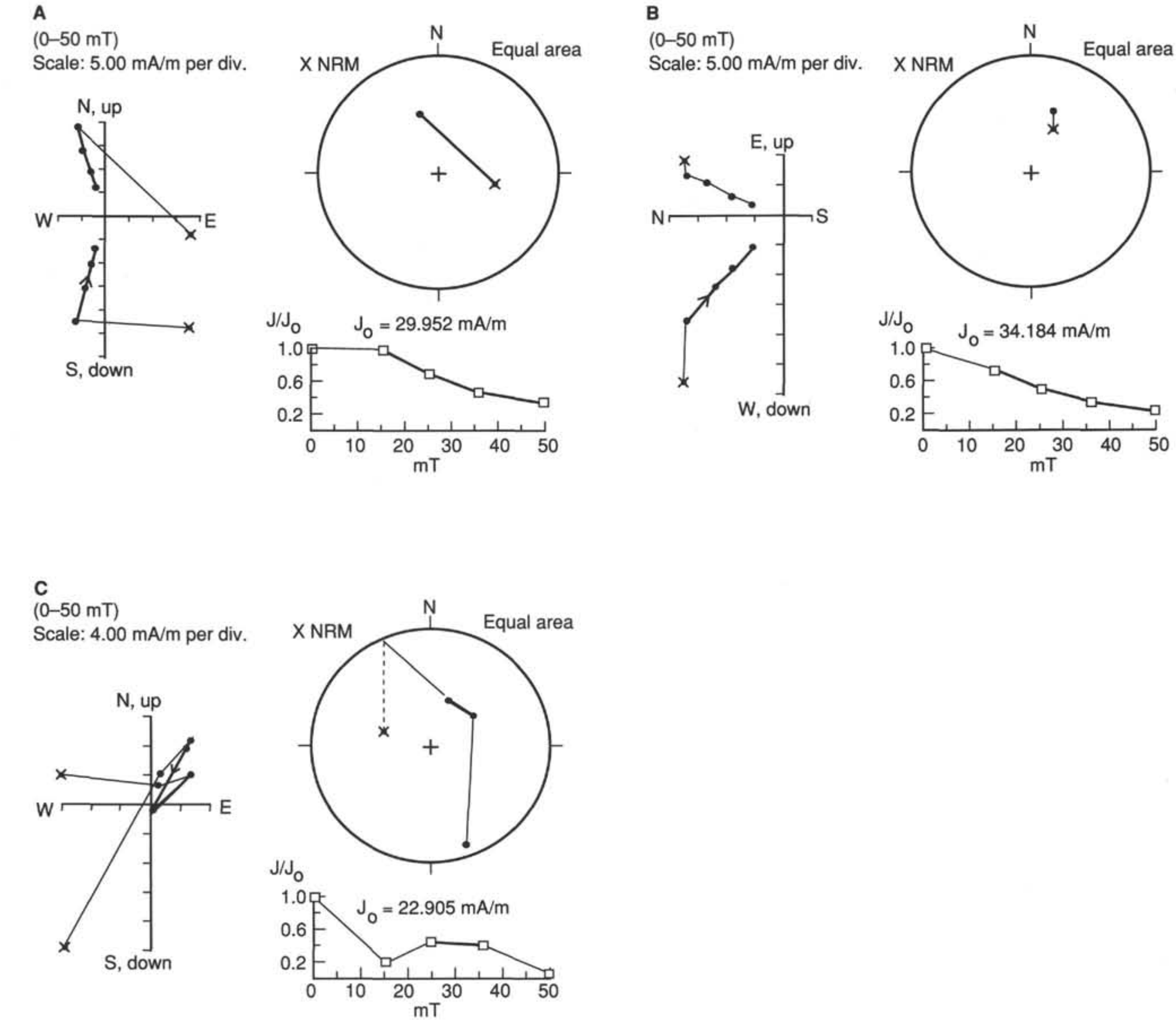

Figure 25. Orthogonal components, field-vector directions, and remanence intensities, as a function of AF demagnetization, for three discrete samples taken from Hole 788D. The heavy lines indicate segments of the AF demagnetization sequence characterized by high directional stability. Negative inclination paths (upper hemisphere) are indicated by a dashed line on the field-vector plots. **A.** Sample 126-788D-5R-1, 15 cm. **B.** Sample 126-788D-10R-1, 30 cm. **C.** Sample 126-788D-15R-1, 38 cm.

Y. Zhang, pers. comm., 1989), for 250-Ka rhyolite lava from a dome atop the en echelon pillow ridges in the Sumisu Rift (Hochstaedter et al., in press), and for dredged rhyolite pumice from the Minami Sumisu submarine caldera (Daisan Sumisu knoll) and another site east of it on the arc (Ikeda and Yuasu, 1989). All pumices were scrubbed, treated several times with ultrasound in deionized water, dried, and handpicked to ensure freshness.

The andesite is similar to the most-differentiated sample from Tori Shima with respect to Si, Mg, and Na. However, it has fractionated more plagioclase, resulting in almost 50% greater iron enrichment (higher Fe, Ti, and V) and lower Al and Ca. Relative to SiO_2, its K, Rb, and Y are about 20%–30% higher than at Tori Shima, whereas its Ba is that much lower in concentration. If confirmed by post-cruise work, this difference in incompatible elements may indicate progressive enrichment of the Izu-Bonin arc in subduction-related incompatible elements during the Pliocene-Quaternary. The Eocene lavas of the outer arc high and the basement lavas at Site 792 are known to have even lower concentrations (see Fryer, Pearce, Stokking, et al., 1990, "Igneous Geochemistry" sections, Sites 781 and 782 chapters). Thus, progressive enrichment in subduction-related incompatible elements through time may characterize the entire Cenozoic history of the arc.

All analyzed Quaternary rhyolite pumices from Sites 788, 790, 791, and 792 are from arc rather than backarc volcanoes. That is, all have lower concentrations of Rb, Zr, Nb, Ce, and Y relative to SiO_2 than do rift rhyolites. In part, this is because the pumices are less differentiated (i.e., they have higher Ti, Fe, Mg, Ca, and P). However, they also have arc-like ratios of incompatible trace elements that the backarc rhyolites lack (e.g., Ba/Zr ~2 rather than 0.5. (REE patterns also should differ, but concentrations even in the rhyolites are too low for shipboard Ce analyses to be sufficiently reliable.)

Indeed, the pumices are extremely depleted in incompatible elements for rhyolitic rocks (e.g., 0.6%–1.0% K_2O and 80–100

Table 8. Shipboard X-ray fluorescence analyses of pumices from Sites 788, 790, 791, and 792.

Site	791A	790B	790B	791A	790C	791B	788C	792B	788C	T88	1888-4	D965-2	D966-1
Section, interval (cm)	3H-3, 0–150	7H, 0–40	10H, 80–150	22H-2, 26–28	5H-1, 0–150	9R-CC, 2–3	12H-5, 10–13	1H-3, 30–31	14H-CC, 5–15				
Lith. unit	Pumice I	Pumice II	Pumice III	Pumice III	Pumice IV	Lith I	Lith IA	Lith I	Lith IA	Tori Shima	Sumisu Rift	Minami Sumisu	Arc
Rock type	Pumice	Pumice	Pumice	Pumice	Pumice	Pumice	Pumice	Pumice	Scoria	Andesite	Rhyolite	Pumice	Pumice
Chemical type	B	A	A	A	B	B	A	A				A/B	B
SiO_2	71.45	70.76	72.55	69.58	73.38	73.08	72.4	69.9	60.86	61.05	72.71	70.65	75.22
TiO_2	0.43	0.56	0.6	0.62	0.48	0.4	0.52	0.62	0.93	0.59	0.39	0.49	0.32
Al_2O_3	13.42	13.66	13.35	13.94	13.16	13.36	13.04	13.9	14.38	15.03	14.65	14.57	13.28
Fe_2O_3*	3.79	4.22	3.84	4.8	3.74	3.55	3.62	4.91	10.54	7.74	2.81	3.88	2.23
MnO	0.11	0.14	0.15	0.14	0.12	0.13	0.12	0.14	0.18	0.16	0.18	0.14	0.09
MgO	0.8	1.02	0.79	1.1	0.86	0.84	1.14	1.06	3.6	3.97	0.28	0.9	0.42
CaO	2.27	3.88	3.54	4.07	3.12	2.98	3.15	4.09	6.51	7.72	1.93	3.61	2.65
Na_2O	5.42	5.17	4.3	4.44	4.18	4.97	4.5	4.46	3.16	3.09	5.93	4.06	3.96
K_2O	1.29	0.75	0.63	0.77	0.87	0.91	1.02	0.76	0.62	0.48	1.03	0.91	1.22
P_2O_5	0.08	0.11	0.1	0.14	0.09	0.07	0.1	0.14	0.11	0.09	0.05	0.11	0.04
LOI	2.11	3.8	2.96	4.25	3.72	0.38	3.89	3.63	1.84		1.64	0.76	5.02
Sum	99.06	100.26	99.9	99.59	99.98	100.29	99.6	99.99	100.9	99.96	99.78	99.32	99.43
(ppm)													
Rb		9.7	6.6	7.8		9.9	10.5		8		23		
Sr		172	169	176		162	144		160	161	132		
Ba		162	155	161		162	116		73	110	150		
Zr		86	83	80		92	112		60	56	291		
Nb		2.7	3.7	3.1		1.3	1.8		1.5		4.5		
Ce		25	29	18		11	13			7.8	39		
Y		44	45	44		47	46		32	23	69		
Ni		0	0	0		1	0		3	12	5		
Cr		0	0	0		0	0			45	1		
V		12	28	34			17		236	186	6		
Zn		114	125	124		112	96		152				
Cu		8	9	5		4	8		40	77			

Note: The stratigraphic unit is either one of the pumice units from within Unit I of Sites 790/791 or a lithologic unit from the site (see "Lithostratigraphy and Accumulation Rates" section, this chapter). The chemical type (A or B) refers to the extent of differentiation (see text). Columns 11–14 are surface samples from the arc and backarc, for comparison (see text for references). LOI = loss on ignition.

ppm Zr at 70%–73% SiO_2) and similar to those described as abundant "quartz keratophyres" in ancient arc terranes (e.g., Brouxel et al., 1987). These very low concentrations, together with the apparent bimodality of volcanism (basaltic andesite plus rhyolite), suggest an anatectic origin for the rhyolites. However, thorough evaluations of similar young bimodal suites in arcs (e.g., Stork and Gill, in press) and backarcs (e.g., Hochstaedter et al., in press) usually show no differences in isotope or trace element ratios between rhyolites and coeval mafic rocks, leaving the nature of their genetic link ambiguous.

There is a range of differentiation among the rhyolites. Based on shipboard study, they are roughly divided into two categories, as shown in Tables 8 and 9, with Type B being more differentiated than Type A. Unfortunately, most Type B pumice clasts are <5 mm in diameter so that shipboard sampling gave insufficient mass for trace element analysis by XRF. All pumice clasts that we encountered were too small for thin sections to be made from the analyzed samples. The six thin sections that have been made of Pliocene-Pleistocene pumices indicate no variation in the phenocryst assemblage of plagioclase-clinopyroxene-orthopyroxene-oxide. However, the differences in chemical composition between Types A and B are similar in magnitude to those among the voluminous 7-Ma, low-K rhyolites in Fiji, which also presage-backarc basin initiation and have differences in phenocryst assemblages (Stork and Gill, in press).

Rhyolite geochemistry and mineralogy may have stratigraphic utility. Except for the rhyolite from Site 792 for which a precise age is unknown, the samples are listed in apparent stratigraphic sequence in Table 8. The first five are from the pumice units that punctuate Unit I of Sites 790 and 791 at roughly 60-Ka intervals (see "Lithostratigraphy and Accumulation Rates" sections, "Sites 790/791" chapter, this volume), whereas the sixth underlies them. The two samples from pumice Unit III belong to chemical Type A. The few differences between them (in Si, Fe, and Mg) make the sample from Site 790 atypical of Type A (i.e., more differentiated). This pumice was pure white, whereas some of the Unit III pumices from Site 791 were visibly mixed, with gray lenses mixed into a white host. Thus, although there are differences among the pumices that are broadly correlative between sites, the occurrence of mingled magma eruptions may damp out the stratigraphically useful geochemical contrasts. The Pliocene pumice from Site 788 differs from the others in some of the same ways the Pliocene andesite differs from the Quaternary andesites (e.g., it has lower concentrations of Ba despite higher Rb).

Table 9. Summary of differences between rhyolite types A vs. B.

Oxide	Type A	Type B
SiO_2	69–73	73–74
TiO_2	0.5–0.6	0.4–0.5
Fe_2O_3	3.8–5.0	3.6–3.8
MgO	1.0–1.2	0.8–0.9
CaO	3.5–4.1	2.3–3.1
Na_2O	4.3–4.5	5.0–5.5
K_2O	0.6–0.8	0.9–1.3
P_2O_5	0.10–0.14	0.07–0.09
Zr (ppm)	80–90	>90
Y	44–46	>46

The two oldest Quaternary pumices are the most differentiated (Type B), whereas pumice Units II and III are more mafic (Type A). Were these from one caldera, it might indicate eruption of increasingly mafic rhyolite from the arc as the new episode of explosive volcanism developed in the late Quaternary. This temporal sequence is common in rhyolitic calderas. The sequence also occurs in low-K arc rhyolite volcanoes, (e.g., Usu, though over much smaller volumes and shorter time scales).

The most recent pumice reverses the "trend," becoming more differentiated again. It is similar in composition to one pumice dredged from the Minami Sumisu submarine caldera (Daisan Sumisu knoll), but pumices from that caldera, and from the arc generally, are diverse and have been studied only in reconnaissance fashion (Table 8). Nonetheless, the volcanic component in the upper Neogene stratigraphic section at all sites of Leg 126 is dominated by rhyolitic pumice. Their stratigraphic variations and origin will be difficult to decipher but are pivotal to understanding the history of Izu-Bonin arc volcanism. In turn, this history is relevant to most ancient arcs in which "quartz keratophyres" play a comparably prominent role.

SEDIMENT/FLUID GEOCHEMISTRY

Seven 10-cm long, whole-round samples from Hole 788C were obtained for electrical resistivity measurements, pore-water squeezing, and sediment and fluid analyses.

Sediment Resistivity

Because of the coarse-grained nature of the sediments, the resistivity measurements could not be conducted.

Sediment Geochemistry

Sediments from Site 788 were analyzed on board ship for inorganic carbon, total carbon, nitrogen, and sulfur (see "Explanatory Notes" chapter, this volume). Analytical results are presented in Table 10. The concentration of organic carbon is unusually low throughout the cored interval, varying from less than the detection limit (about 0.01%) to 0.23%. Nitrogen could not be detected in any of the samples. The concentration of sulfur is uniformly low, with an average of about 0.05%.

Fluid Geochemistry

The headspace hydrocarbon analyses did not show any gases above the background level and thus are not reported.

Sodium, strontium, and iron could not be analyzed because of a shortage of acetylene. The composition of the interstitial water is unusually uniform and only shows a slight enrichment of calcium and a depletion of magnesium relative to seawater of similar chlorinity. As one would expect in organic-poor sediments like this, there is no indication of bacterial sulfate reduction. This is further substantiated by the low concentrations of ammonium. However, the elevated manganese and dissolved silicon concentrations (Table 11) clearly distinguish the pore waters from seawater. Thus, despite the coarse-grained nature of the squeezed sediments, the pore waters do not appear to have been appreciably contaminated by seawater. The high concentrations of dissolved manganese show that the subsurface redox conditions are sufficiently low to stabilize Mn(II). Thus, at present, the manganese overgrowths observed in Unit I (see "Lithostratigraphy and Accumulation Rates" section, this chapter) are being remobilized.

Despite the abundance of volcanogenic material, there are no strong signs of low-temperature alteration reactions. This may be related to the coarseness of the sediments, resulting in a small, reactive surface area/water ratio and effective exchange with the overlying seawater.

Table 10. Concentration of organic carbon, total nitrogen, and sulfur in samples from Holes 788C and 788D.

Core, section, interval (cm)	Depth (mbsf)	Inorg C (%)	$CaCO_3$ (%)	Tot C (%)	Org C (%)	Tot N (%)	Tot S (%)
126-788C-							
1H-3, 140-150	8.4	0.06	0.5	0.02	LD	LD	LD
3H-5, 140-150	27.6	0.05	0.42	0.02	LD	LD	0.03
5H-4, 19-21	43.89	0.01	0.08	0.02	0.01	LD	0.04
5H-6, 32-34	47.02	0.02	0.17	0.02	LD	LD	0.09
6H-3, 55-57	52.25	0.01	0.08	0.01	LD	LD	0.08
6H-5, 24-26	54.94	0.02	0.17	0.01	LD	LD	0.07
7H-1, 35-37	58.55	0.01	0.08	0.03	0.02	LD	0.08
7H-1, 140-150	59.6	0.04	0.33	0.03	LD	LD	0.08
7H-2, 23-25	59.93	0.01	0.08	0.01	LD	LD	0.05
8H-1, 81-83	68.51	0.01	0.08	0.01	LD	LD	0.07
8H-2, 90-92	70.1	0.01	0.08	ND	ND	ND	ND
9H-1, 25-27	77.45	0.01	0.08	ND	ND	ND	ND
9H-3, 39-41	80.59	0.02	0.17	ND	ND	ND	ND
9H-3, 140-150	81.6	0.04	0.33	ND	ND	ND	ND
9H-5, 63-65	83.83	0.01	0.08	0.01	LD	LD	0.11
11H-3, 82-85	100.02	0.01	0.08	0.03	0.02	LD	0.09
11H-4, 132-134	102.02	0.01	0.08	ND	ND	ND	ND
11H-5, 11-13	102.31	0.02	0.17	ND	ND	ND	ND
12H-3, 59-61	109.29	0.01	0.08	ND	ND	ND	ND
12H-6, 34-36	113.54	0.01	0.08	0.01	LD	LD	0.05
13H-3, 71-73	118.91	0.02	0.17	0.03	0.01	LD	0.09
13H-5, 69-71	121.89	0.02	0.17	0.03	0.01	LD	0.05
13H-6, 0-10	122.7	0.05	0.42	0.01	LD	LD	0.03
14H-4, 48-50	129.68	0.01	0.08	0.02	0.01	LD	0.07
14H-5, 90-93	131.6	0.01	0.08	0.01	LD	LD	0.05
15H-1, 46-48	134.66	0.02	0.17	0.03	0.01	LD	0.07
16H-1, 89-90	144.59	0.02	0.17	0.04	0.02	LD	0.09
16H-1, 140-150	145.1	0.02	0.17	0.01	LD	LD	0.02
18H-2, 89-90	165.09	0.01	0.08	0.03	0.02	LD	0.07
19H-6, 67-68	180.37	0.02	0.17	0.01	LD	LD	0.04
20H-2, 63-64	183.83	0.01	0.08	0.03	0.02	LD	0.07
21H-1, 17-18	191.37	0.02	0.17	0.04	0.02	LD	0.1
23H-1, 62-64	210.82	0.01	0.08	0.04	0.03	LD	0.08
23H-3, 140-150	214.6	0.02	0.17	0.01	LD	LD	0.02
24H-2, 108-110	222.28	0.02	0.17	ND	ND	ND	ND
126-788D-							
4R-1, 107-109	249.57	3.49	29.07	3.56	0.07	LD	LD
5R-1, 7-8	258.27	4.34	36.15	4.57	0.23	LD	0.07
5R-1, 146-147	259.66	1.75	14.58	1.86	0.11	LD	0.03
8R-1, 14-16	287.34	0.09	0.75	0.1	0.01	LD	0.03
9R-1, 31-33	297.21	0.02	0.17	0.04	0.02	LD	0.04
9R-1, 91-93	297.81	0.14	1.17	0.16	0.02	LD	0.02
10R-1, 21-23	306.71	0.14	1.17	ND	ND	ND	ND
11R-1, 21-23	316.21	0.47	3.92	0.52	0.05	LD	0.04
12R-1, 31-33	325.91	2.39	19.91	2.55	0.16	LD	LD
13R-1, 3-5	335.33	0.07	0.58	ND	ND	ND	ND
15R-1, 42-44	355.12	0.09	0.75	0.1	0.01	LD	0.04
16R-1, 36-38	364.66	0.02	0.17	0.04	0.02	LD	0.04
16R-1, 60-62	364.9	0.99	8.25	1.04	0.05	LD	0.03

Note: LD = less than the detection limit and ND = not determined.

PHYSICAL PROPERTIES

Introduction

Multisensor track (MST) logging, index property, and velocity measurements were made on cores from Holes 788C and 788D. MST logging was suspended following Core 126-788D-9R, and only MST logging measurements were made in Hole 788A. No physical property measurements were made on sediments from Hole 788B or Site 789. The primary lithology of the upper unconsolidated material (Subunit IA) consists of coarse, pumice-rich sediment (see "Lithostratigraphy and Accumulation Rates" section, this chapter) and is particularly susceptible to disturbance. Therefore, no vane shear strength analyses were made and even the index property data should be viewed with caution. The unconsolidated, friable nature of this material made Hamilton Frame velocity measurements impractical and only one measurement was made. No thermal conductivity measurements were made on cores from Sites 788 or 789.

Index Properties

Unit I consists of structureless, pumiceous sandy gravel and is highly disturbed by drilling. Although the most obvious anomalous values are not included in the figures and interpretations, all the data from the pebbly and gravelly intervals are suspect. Nevertheless, it is possible to recognize certain trends in the index property data. More confidence may be placed in data obtained from Unit II, which is finer grained and more consolidated (see "Lithostratigraphy and Accumulation Rates" section, this chapter).

Grain density values display the least downhole variability of the index properties (Table 12 and Fig. 26) and exhibit a slight increase downhole. Grain density values in Unit I range from 2.3 to 2.8 g/cm^3 and average 2.56 g/cm^3. The range in Unit II is from 2.4 to 2.79 g/cm^3, but the average is slightly higher (2.63 g/cm^3). As expected, fewer anomalous values exist in Unit II (Table 12). Unlike the previous three sites (787, 790, and 791), only a weak correlation between grain density values and carbonate contents was observed. A slight increase in mean grain density values from Unit I to Unit II is probably related to the higher average $CaCO_3$ content (in Unit II), but it may also correlate to an increase in heavy minerals, such as olivine and hornblende.

Only five data points remain after filtering and averaging the GRAPE bulk-density measurements made on a single core sec-

Table 11. Composition of pore water for samples from Site 788.

Core, section, interval (cm)	Depth (mbsf)	pH	Alk. (meq/l)	Sal. (g/kg)	Cl^- (mM)	SO_4^{2-} (mM)	Mg^{2+} (mM)	Ca^{2+} (mM)	K (mM)	Li (μm)	Mn (μm)	SiO_2 (μm)	NH_4 (μm)
126-788C-													
1H-3, 140–150	8.45	7.27	2.31	35.5	557	28.3	51.9	11.2	11.3	26.3	53	497	18
3H-5, 140–150	27.65	7.44	2.36	35.5	554	29.7	51.8	11.2	11.0	22.3	58	459	23
7H-1, 140–150	59.65	7.49	2.38	35.0	552	28.9	51.9	11.1	11.3	24.3	60	440	LD
9H-3, 140–150	81.65	7.51	2.48	35.0	557	28.8	52.2	11.5	11.2	24.3	48	518	LD
13H-6, 0–5	122.75	8.03	2.53	35.0	556	29.6	52.1	11.4	10.9	21.6	39	585	LD
16H-1, 140–150	145.15	8.09	2.59	35.0	556	27.9	52.6	11.5	11.0	23.0	30	537	LD
23H-3, 140–150	214.65	7.97	2.50	35.5	556	28.3	52.5	11.4	11.3	23.7	29	495	LD

Note: LD = less than the detection limit.

tion in Hole 788A (126-788A-4R-1). These data agree well with those obtained at similar depths in Hole 788C. A comparison of GRAPE density measurements in Hole 788D with gravimetrically derived values (Fig. 27) further illustrates the previously reported problems associated with GRAPE data from rotary-drilled sections. The two data sets are nearly mirror images of each other. This, along with other data from Sites 787, 790, and 791 (see "Physical Properties" sections, Sites 787 and 790/791 chapters), is enough evidence to suspend any further acquisition of GRAPE data on rotary-drilled sections. Consequently, only GRAPE density data from Hole 788C (i.e., Unit I) are discussed here.

GRAPE and gravimetric bulk densities in Hole 788C (Unit I) correlate reasonably well despite the high degree of disturbance and poor sample quality within this unit (Fig. 27). However, several gravimetric values fall significantly below the curve of GRAPE density. Introduction of additional water into these core sections during the splitting process may contribute to these low bulk density values.

Variability in both types of density measurements is noted at scales of approximately 10–30 m. Preliminary comparisons with the lithostratigraphy (see "Lithostratigraphy and Accumulation Rates" section, this chapter) suggest that the higher bulk density values are associated with vitric sand and silt layers. Furthermore, these sediments may contain large amounts of dense, mafic minerals.

Gravimetrically determined wet-bulk density values generally exhibit a significant degree of scatter. However, the Unit I/II boundary is well defined on the basis of a sharp increase in bulk density from an average of 1.48 g/cm^3 in Unit I to an average of 1.96 g/cm^3 in Unit II. Despite the poor quality and scatter of the data in Unit I, this change is distinct and obvious. The primary cause of this density increase is thought to be the transition from unconsolidated to lithified material (see "Lithostratigraphy and Accumulation Rates" section, this chapter). Unfortunately, because of very low recovery in Subunit IB, no physical property samples were obtained in this unit. Therefore, the boundary between these two consolidation states is not well defined.

Sharp changes are also observed in the porosity and water content data. Unit I is characterized by fairly constant to slightly increasing downhole trends with mean values of 72.8% (porosity) and 105% (water content). The wide range of values in both parameters (50.8%–89.1% and 32.2%–178%, in porosity and water content, respectively) is probably the result of drilling disturbance. Porosity values in Unit II are much lower, averaging 60%; water contents average 52%. A fair amount of scatter in the values persists. This scatter most likely results from sampling different lithologies, specifically vitric sand and siltstones vs. nannofossil-rich claystones.

Calcium Carbonate

Calcium carbonate contents in the upper 249 m (Unit I) never exceed 0.5%, and most values are <0.2% (Fig. 26). An increase to values as high as 36% occurs in Unit II. Two distinct layers with high carbonate contents, centered at 258 and 326 mbsf, consist of nannofossil-rich claystones (see "Lithostratigraphy and Accumulation Rates" section, this chapter). The remainder of Unit II is composed of sediment with carbonate contents comparable to those in Unit I.

Sonic Velocity

Hamilton Frame velocity measurements are shown in Figure 26 and are compared with MST *P*-wave logger results in Figure 28. Within Unit I, the coarse, unconsolidated, pumiceous nature of the majority of the sediments (see "Lithostratigraphy and Accumulation Rates" section, this chapter) allowed only one Hamilton Frame velocity measurement on a vitric silt unit. The resulting velocity of 1.60 km/s is in close agreement with MST velocity measurements at this depth (Fig. 28). MST velocity values within Unit I average 1.58 km/s and range from 1.56 to 1.62 km/s. These velocity data should be viewed with caution because of coring disturbances in these unconsolidated sediments.

Velocity measurements in Unit II are significantly higher than in Unit I. Hamilton Frame velocity values in Unit IIA average 2.68 km/s and range from 2.37 to 3.29 km/s (Table 12 and Fig. 26). This distinct increase in velocity, as well as in index property data, between Units I and II indicates a significant difference in the degree of consolidation between these units.

Within Subunit IIB, velocity data averaged 2.79 km/s and ranged from 2.00 to 3.46 km/s. These faster velocities are probably a result of increased consolidation caused by increased overburden, as well as the greater amount of coarse sediments (see "Lithostratigraphy and Accumulation Rates" section, this chapter).

REFERENCES

Berggren, W. A., Kent, D. V, Flynn, J. J., and Van Couvering, J. A., 1985. Cenozoic geochronology. *Geol. Soc. Am. Bull.*, 96:1407–1418.

Berner, R. A., 1981. A new geochemical classification of sedimentary environments. *J. Sediment. Petrol.*, 51:359–365.

Bernhard, J. M., 1986. Characteristic assemblages and morphologies of benthic foraminifera from anoxic, organic-rich deposits: Jurassic through Holocene. *J. Foram. Res.*, 16:207–215.

Bolli, H. M., Saunders, J. B., and Perch-Nielsen, K. (Eds.), 1985. *Plankton Stratigraphy*: Cambridge (Cambridge Univ. Press).

Brouxel, M., Lapierre, H., Michard, A., and Albarede, F., 1987. The deep layers of a Paleozoic arc: geochemistry of the Copley-Balaklala series, northern California. *Earth Planet. Sci. Lett.*, 86:386–400.

Fryer, P., Pearce, J. A., Stokking, L., et al., 1990. *Proc. ODP, Init. Repts.*, 125: College Station, TX (Ocean Drilling Program).

Hochstaedter, A. G., Gill, J. B., Newman, S., Pringle, M., Taylor, B., and Fryer, P., in press. Volcanism in the Sumisu Rift I: The effect of distinctive volatiles on fractionation. *Earth Planet. Sci. Lett.*

Ikeda, Y., and Yuasu, M., 1989. Volcanism in Nascent back-arc basins behind the Shichito Ridge and adjacent areas in the Izu-Ogasawara arc, Northwest Pacific: evidence for mixing between E-type MORB and island arc magmas and the initiation of backarc rifting. *Contrib. Mineral. Petrol.*, 101:377–393.

Ingle, J. C., Jr., 1980. Cenozoic paleobathymetry and depositional history of selected sequences within the southern California continental borderland. *Spec. Publ. Cushman Found. Foraminiferal Res.*, 19: 163–195.

Odin, G. S., and Matter, A., 1981. Die glauconarium origine. *Sedimentology*, 28:611–643.

Okada, H., and Bukry, D. 1980. Supplementary modification and introduction of code numbers to the "Low-latitude coccolith biostratigraphic zonation" (Bukry, 1973; 1975). *Mar. Micropaleontol.*, 5: 321–325.

Perch-Nielsen, K., 1985. Cenozoic calcareous nannofossils. *In* Bolli, H. M., Saunders, J. B., and Perch-Nielsen, K. (Eds.), *Plankton Stratigraphy*: Cambridge (Cambridge Univ. Press), 427–554.

Stork, A. L., and Gill, J. B., in press. Low-K rhyolites and high-Mg andesites accompany the early stages of backarc basin formation in the southwest Pacific, *J. Geol.*

Taylor, B., Brown, G., Fryer, P., Gill, J., Hochstaedter, A., Hotta, H., Langmuir, C., Leinen, M., Nishimura, A., and Urabe, T., in press. ALVIN-SeaBeam studies of the Sumisu Rift, Izu-Bonin Arc. *Earth Planet. Sci. Lett.*

Usui et al., 1987. Local variability of manganese nodules facies on small abyssal hills of the Central Pacific Basin. *Mar. Geol.*, 74:237–276.

Van Morkhoven, F.P.C.M., Berggren, W. A., and Edwards, A. S., 1986. Cenozoic cosmopolitan deep-water benthic foraminifera. *Bull. Cent. Rech. Explor.-Prod. Elf-Aquitaine, Mem.*, No. 11.

Weissel, J. K., and Karner, G. D., 1989. Flexural uplift of rift flanks due to tectonic denudation of the lithosphere during extension. *J. Geophys. Res.*, 94:13913–13950.

Woodruff, F., 1985. Changes in Miocene deep-sea benthic foraminiferal distribution in the Pacific Ocean: relationship to paleoceanography. *In* Kennett, J. P. (Ed.), *The Miocene Ocean: Paleoceanography and Biogeography.* Mem. Geol. Soc. Am., 163:131–175.

Yasuda, H., 1989. Benthic foraminifers and sedimentary facies of the lower slope basin off Shikoku, Japan. *In* Takayanagi, Y., and Ishizaki, K. (Eds), *Collected Papers on Foraminifera from the Japanese Islands*: Sendai (Toko Press), 83–92.

Ms 126A-107

NOTE: All core description forms ("barrel sheets") and core photographs have been printed on coated paper and bound as Section 3, near the back of the book, beginning on page 421.

Table 12. Physical property data of samples from Holes 788C and 788D.

Core, section, interval (cm)	Depth (mbsf)	Wet-bulk density (g/cm³)	Dry-bulk density (g/cm³)	Porosity (%)	Water content (%)	Grain density (g/cm³)	Void ratio	Carbonate content (%)	Velocity (km/s)
126-788C-									
1H-3, 75–76	7.75	1.57	0.94	64	71	2.42	1.77	0.5	
3H-3, 87–88	24.07	1.52	0.85	68	84	2.46	2.12	0.4	
4H-2, 113–115	32.33	1.50	0.85	66	82	2.22	1.92		
4H-4, 40–41	34.60	1.42*	0.63*	79*	135*	2.52*	3.85*		
5H-4, 20–21	43.90	1.71	1.15	57	52	2.39	1.31	0.1	
5H-6, 32–34	47.02	1.32	0.51	82	175	2.42	4.60	0.2	
6H-3, 57–59	52.27	1.39	0.67	73	116	2.56	2.69	0.1	
6H-5, 26–28	54.96	1.33	0.71	63	93	3.34	1.68	0.2	
7H-1, 36–38	58.56	1.35	0.54	82	163	2.51	4.42	0.1	
7H-1, 140–150	59.60							0.3	
7H-2, 24–26	59.94	1.16	0.49	68	148	1.89	2.10	0.1	
8H-1, 81–83	68.51	1.48	0.61	88	157	1.93	7.49	0.1	
8H-2, 91–93	70.11	1.64	0.99	65	69	2.65	1.87	0.1	
9H-1, 26–28	77.46	1.59	0.95	65	72	2.52	1.85	0.1	
9H-3, 40–41	80.60	1.40	0.62	79	138	2.31	3.76	0.2	
9H-3, 140–150	81.60								
9H-5, 63–66	83.83	1.37	0.58	80	150	2.59	4.10	0.1	
11H-3, 82–84	100.01	1.50*	0.80*	71*	95*	2.54*	2.49*	0.1	1.6
11H-4, 132–133	102.02	1.99*	1.11*	89*	85*	2.51*	8.16*	0.1	
11H-5, 11–12	102.31	1.63*	0.97*	66*	71*	2.56*	1.94*	0.2	
12H-3, 60–63	109.30	1.38	0.80	78	139	2.59	3.58	0.1	
12H-6, 35–37	113.55	1.54	0.68	68	82	2.47	2.12	0.1	
13H-3, 70–72	118.90	1.52	0.81	71	91	2.50	2.39	0.2	
13H-5, 70–72	121.90	1.58	1.00	64	71	2.45	1.79	0.2	
13H-6, 0–10	122.70							0.4	
14H-4, 48–50	129.68	1.43	0.66	78	125	2.80	3.44	0.1	
14H-5, 92–94	131.62	1.62	0.89	65	69	2.54	1.84	0.1	
15H-1, 46–48	134.66							0.2	
16H-1, 90–92	144.60	1.42*	0.41*	81*	140*	2.69*	4.26*	0.2	
16H-1, 140–150	145.10							0.2	
17H-4, 112–114	158.82	1.57	0.91	77	102	2.54	3.35		
18H-2, 90–92	165.10	1.52	0.95	76	106	2.72	3.19	0.1	
19H-6, 67–69	180.37	2.13	1.65	51	32	2.80	1.03	0.2	
20H-2, 63–65	183.83	1.59	0.87	71	85	2.55	2.45	0.1	
21H-1, 16–18	191.36	1.61	0.63	72	84	2.75	2.57	0.2	
23H-1, 62–64	210.82	1.39	0.77	82	152	2.69	4.61	0.1	
24H-2, 106–108	222.26	1.35	0.52	84	178	2.72	5.30	0.2	
126-788D-									
1R-1, 9–11	219.69	1.68	0.7	80	94	2.47	3.90		
4R-1, 109–111	249.59	2.12	1.32	95	85	2.27	18.46	29.1	2.58
5R-1, 7–8	258.27							36.2	
5R-1, 143–145	259.63	2.11	1.52	47	30	2.40	0.88	14.6	3.29
5R-2, 16–19	259.86	1.95	1.4	55	40	2.72	1.22		2.76
6R-1, 35–37	268.26	1.86	1.31	58	46	2.60	1.35		2.37
7R-1, 92–94	278.42	1.88	1.33	49	37	2.52	0.97		2.94
7R-2, 32–34	279.32	1.92	1.38	51	38	2.59	1.05		2.39
8R-1, 0–2	287.20	1.68	1.25	64	64	2.27	1.76		
8R-1, 1–2	287.21	1.68		64	64	2.49	1.79		
8R-1, 14–16	287.34	2.03	1.77	62	46	2.73	1.65	0.8	2.51
9R-1, 31–33	297.21							0.2	
9R-1, 89–91	297.79	2.19	1.44	48	29	2.72	0.91	1.2	3.06
10R-1, 21–23	306.71	2.47	1.26	45	23	2.69	0.83	1.2	3.46
11R-1, 20–22	316.20	1.76	1.66	73	73	2.72	2.64	3.9	2.04
12R-1, 30–33	325.90	1.91	1.21	64	53	2.79	1.81	19.9	2.64
13R-1, 5–6	335.35	1.84	1.2	59	49	2.57	1.46	0.6	2.65
14R-1, 12–14	345.12	2.00	1.83	55	39	2.43	1.20		
15R-1, 42–46	355.12	1.97	1.27	52	37	2.75	1.06	0.8	2.80
16R-1, 36–38	364.66	1.80		61	53	2.62	1.55	0.2	2.61
16R-1, 58–60	364.88	2.21	1.95	51	31	2.75	1.02	8.3	2.88

Note: Asterisks (*) mark measurements from finer grained, more consolidated beds that are considered more accurate values than those from the coarse, pumiceous sediments in the upper 230 mbsf. Other data are suspect.

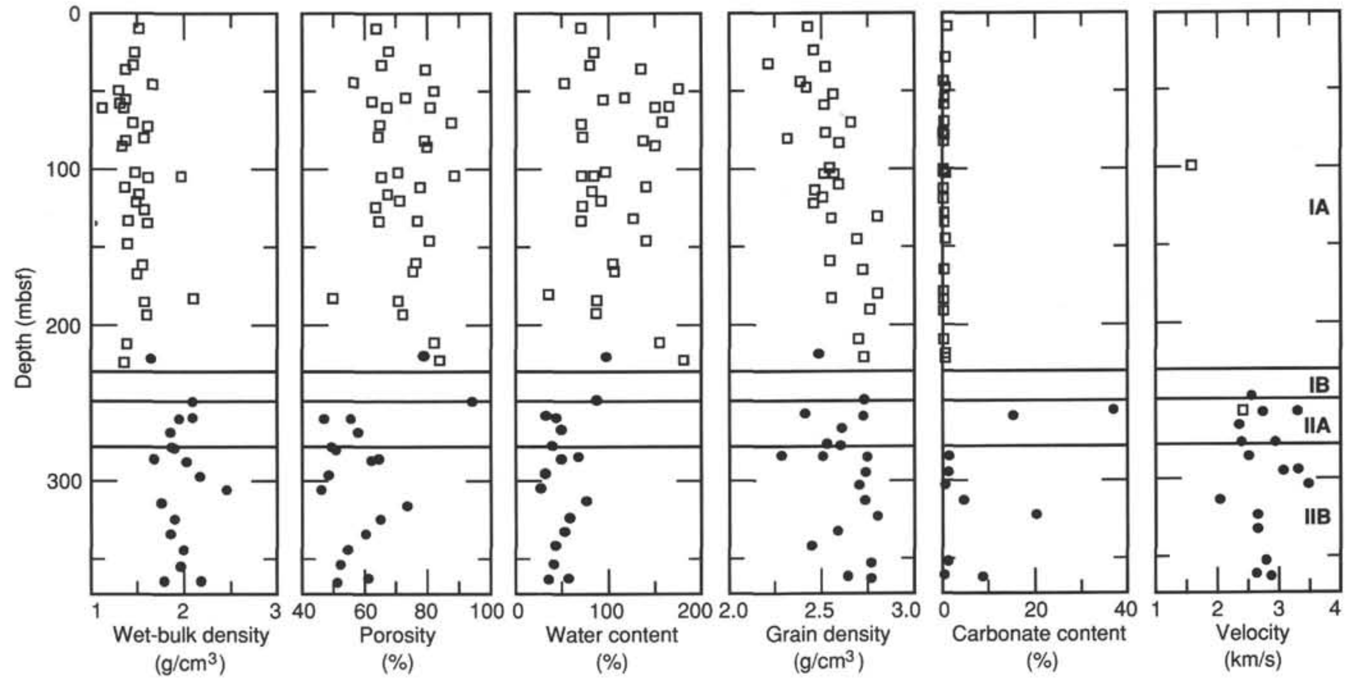

Figure 26. Physical property data from Site 788, Holes 788C (open squares) and 788D (solid circles). Locations of lithostratigraphic unit boundaries are indicated.

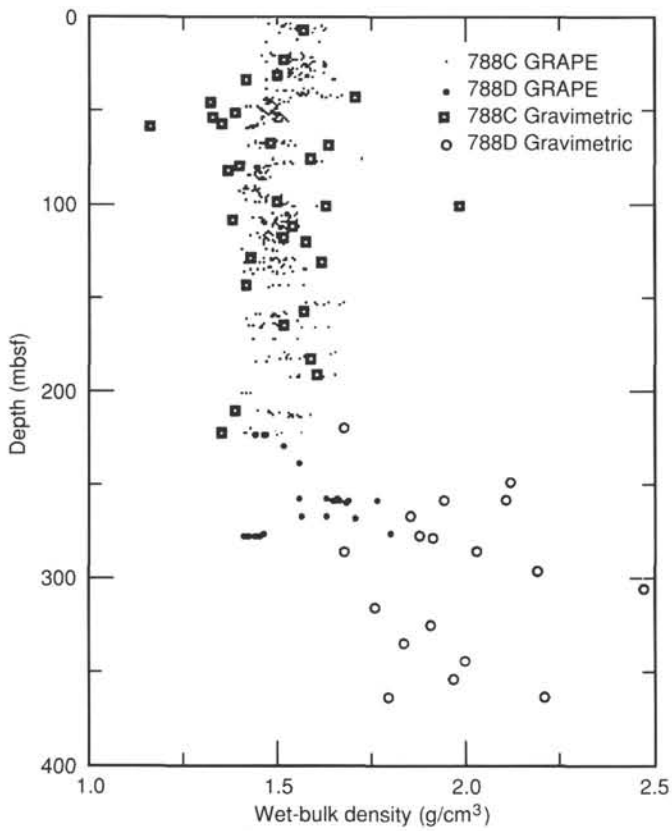

Figure 27. GRAPE and gravimetric wet-bulk density values from Holes 788C and 788D.

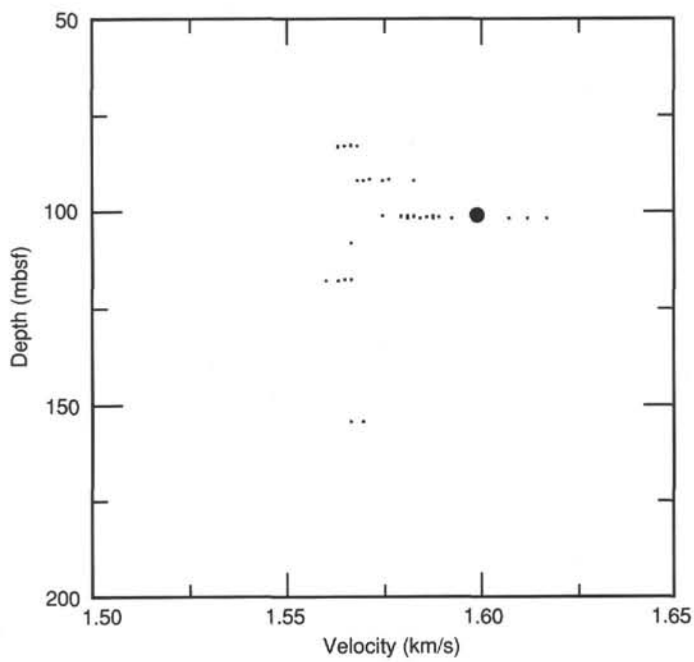

Figure 28. Comparison of Hamilton Frame (solid circle) and multisensor track *P*-wave logger (small points) analyses on sediments from Hole 788C.